4 RESULTS

This chapter describes the results obtained using the methodologies of Chapter 3. It includes images reconstructed from data acquired by the experimental system described in Chapter 2, but it also includes results obtained from data simulated using the methodology presented in Section 3.4.

4.1 Simulations

This section describes and discusses reconstructed images from simulated data. The way the data are simulated is described in Section 3.4. The algorithms used to reconstruct the images are the same for both simulated and experimental data. This is very convenient to compare simulations and experiments.

In all of the simulations the transmitter and receiver were point transmitter and point receiver. This approximation does not have important consequences because the experimental devices also have a mostly spherical beampattern, due to their λ/a ratio at the frequency of operation. Moreover, this approximation allows us to shorten the time necessary to simulate the signals.

Also in all the simulations, a two-cycle, 2-kHz pulse was used. This was done to match the pulse used in the experiments. All the simulations assumed a speed of propagation of 200 m/s and an attenuation of 0.6 dB/kHz/cm, because these are the values experimentally measured as shown in Section 2.2. Finally, all the targets are perfect point targets, which means they have a reflection coefficient of unity.

4.1.1 Single target in a pulse-echo mode simulation

This is one of the simplest simulations that can be accomplished. It is the case where a single point target is put into the medium, and the receiver and transmitter are assumed to be located at the same position.

In our case the scan is composed of 51 points, with a step size of 1 cm. The 3-D grid is a cube with a sidelength of 50 cm, sampled in the three directions every centimeter. The target is buried at a depth of 25 cm, in the middle of the sand box. The parameter and scatterer files corresponding to this simulation are shown in Appendix C.1.

The reconstructed image using the beamformer.m script (description in Section 3.3 and code in Appendix 5.3.2) is in Figure 4.1. This figure shows that a single target already creates a significant pattern on the reconstructed image. It is 45 cm wide and 20 cm long. One can also clearly see the two cycles of the excitation pulse with the first cycle generating a high intensity at a depth of 28 cm and the second one at a depth of 36 cm.

This image is interesting because it gives us an idea of what to expect in terms of resolution. The axial resolution is clearly related to the length of the pulse. The lateral resolution is more related to the decay of the echo from the target when the source/receiver is moving farther away from the target.

It is also important to understand that this image is already in focus at all depths because the transmitter and receiver are located at the same position. Hence, the use of dynamic focusing (DF) would yield the same picture. The use of TGC is also unnecessary because in this first simulation we just included a single target.

Actually, this picture shows the pattern created by a single ideal point reflector. Therefore Figure 4.1 can be interpreted as displaying the point-spread function of the imaging system. Knowing the point-spread function of the system is not only important for resolution considerations as discussed above, but it can also help reconstruct better images. One could try to deconvolve the image with the point-spread function, which would lead in the ideal case to a perfect reconstruction. That is a single point for each target.

4.1.2 Time gain compensation validation

The goal of this simulation was to validate the inclusion of time gain compensation TGC into the reconstruction technique. The geometry of the scan is exactly the same as the one described in Section 4.1.1; in particular we are still using a pulse-echo mode. The difference is that in this case we have five point targets instead of one as before. They have all the same x and y coordinates, but the targets were buried at different depths: 0.05 m, 0.15 m, 0.25 m, 0.35 m, and 0.45 m. The parameter and scatterer files corresponding to this simulation are shown in Appendix C.2.

Figure 4.2 was reconstructed without the use of TGC, whereas in Figure 4.3 TGC was used. TGC allows us to see all the targets, whereas without

TGC only one target can be seen. Figure 4.2 appears to show two targets but it is actually the two cycles of the 0.05-m-deep target that are seen. The 0.15-m-deep target echo signal amplitude is already more than 30 dB below the 0.05-m-deep target echo signal amplitude.

In Figure 4.3 the five targets seem to be visible but not at the correct depths. The 0.05-m-deep target seems to appear at 0.08 m, and the 0.15-m-deep target seems to appear at 0.12 m or so. Actually, the targets are visible at the correct depths. But, for example, the 0.05-m-deep target has a very low amplitude echo. This is due to TGC: when the two-cycle pulse hits the target and bounces back it generates two cycles, but the second cycle arrives after the first cycle; hence TGC gives to the second cycle a higher amplitude than to the first cycle. For example, what we see at a depth of around 0.12 m is not the echo from the 0.15-m-deep target, but the amplified second cycle of the echo from the 0.05-m-deep target. In medical imaging a weaker TGC is sometimes used [1] so that structures present at small depths are not masked by compensated structures present deeper.

Figure 4.3 also shows a drawback of TGC. The point targets have much bigger side patterns than without the use of TGC. This means that the point target generates larger echos away from the target than without the use of TGC.

4.1.3 Delay-and-sum beamforming simulations

In the following simulations the targets were the same as in Section 4.1.2. Five targets are in the middle of the box at depths: 0.05 m, 0.15 m, 0.25 m, 0.35 m, and 0.45 m.

On receive an eight-element line array was simulated. The line array was along the direction of the scan and the elements were 1.8 cm apart. If we refer to the parameter file (Section 3.4.3), it means that Nx=8 and Ny=1. The spacing between elements was 1.8 cm. The parameter and scatterer files corresponding to that simulation are shown in Appendix C.3.

Figures 4.4, 4.5, 4.6, and 4.7 show reconstructed images. Following are the techniques used to reconstruct them:

- Figure 4.4: DF used without smoothing, and without TGC.
- Figure 4.5: DF used without smoothing, and with TGC.
- Figure 4.6: DF used with smoothing, and without TGC.
- Figure 4.7: DF used with smoothing, and with TGC.

For all four figures DF was accomplished using 20 discrete depths of focus on a range of 50 cm. This means that the signals were focused every 2.5 cm. Moreover, because λ =10 cm, signals were focused every $\lambda/4$.

Figures 4.4 and 4.5, reconstructed without smoothing, are shown to demonstrate the necessity of smoothing the final image when using dynamic focusing. One can easily see in Figures 4.4 and 4.5 discontinuities of the images at the depths where focused signals are concatenated (for example, at a depth of 0.1 m). Smoothing was done using the technique described in Section 3.2.2. From now on all the images reconstructed using DF will be reconstructed using smoothing as well.

Figures 4.2 and 4.6 look similar. The differences are mostly in the relative energy levels of the targets. This means that the targets show almost the same shapes on the reconstructed images but they have a higher amplitude when DF was used. Specifically, Figure 4.6 allows us to see the 0.15-m-deep target and even the 0.25-m-deep target, whereas in Figure 4.2 only the first target is seen.

Figures 4.3 and 4.7 also look similar. The use of TGC allows us to see all targets on both, but when DF is used the targets have a higher amplitude as the depth increases. For example, the target seen at depth 0.45 m in Figure 4.3 has a relative intensity of -15 dB, whereas in Figure 4.7 its relative intensity is of -8 dB.

The higher intensity seen on images using DF (Figures 4.6 and 4.7) compared to the images where DF was not used (Figures 4.2 and 4.3) is due to the fact that DF basically makes the signals arrive in phase at almost every depth. And, in phase signals yield a higher amplitude than out-of-phase signals.

The use of TGC also increases the effect of DF. The differences in amplitude are more visible when comparing Figures 4.3 and 4.7 than when comparing Figures 4.2 and 4.6. This means that enhancements due to DF are more important at lower depths that only TGC permits us to see.

4.2 Experimental Images

This section presents some of the images reconstructed using the techniques of Chapter 3 with data acquired by the experimental system described in Chapter 2.

4.2.1 Targets

Figure 4.8 shows the targets that were used in the experiments. The big steel plate is 40 cm x 40 cm x 2 cm, and the small plates are 1.2 cm x 7.5 cm x 60 cm. In the picture the ruler is 50 cm long and 3 cm wide.

4.2.2 B-mode images

For all the B-mode images presented in this section, the transmitted pulse was a 2-kHz, two-cycle sine wave. The peak-to-peak voltage going into the MST was 300 V. The step size was equal to 1 cm. In the following scans no arrays were simulated, meaning that a single signal was acquired at each step of the scan. Actually 32, signals were averaged at each position with a pulse repetition frequency (PRF) of 10 Hz. Then MST moved to the next position. The distance between MST and Terr was kept constant and equal to 23 cm. This simple scan geometry is shown in Figure 4.9.

Figure 4.10 shows a B-mode image where the target was the big steel plate (Figure 4.8) buried at a depth of 10 cm. The target is located in the middle of the scan, and because the target is 40 cm wide, its borders can be seen in Figure 4.10 at horizontal positions of 0.18 cm and 0.62 cm. Therefore, the shape on the picture is 4 cm wider than the target. This is due to the omnidirectonal transducers. Terr is therefore acquiring echoes from the target even when the two transducers are not above the target.

This figure clearly shows that there is a target present in the box. However, on the left side of the figure between horizontal distances of 0 and 0.1 m, an important artifact is present staring at a depth of around 12 cm and finishing at a depth of around 45 cm. Since this artifact is essentially present only on the left side of the image, it might be due to a reflection coming from the sides of the box. Figure 4.10 also shows the limited axial resolution. The steel plate is only 2 cm, but the echo coming from the target is starting at 0.1 m and finishing at 0.33 m, that is, 23 cm long. This is because the pulse is composed of two cycles at 2 kHz, making it 2λ =20 cm long in the range direction.

Figure 4.11 describes the shape made by four small plates stacked together and all touching each other. This configuration was buried into the sand. The B-mode image obtained is in Figure 4.12. The result is similar as the one obtained in Figure 4.10. The target can be seen, but generates an important shape due to the length of our 2-kHz, two-cycle pulse. The only difference is the presence of artifacts on both sides, whereas nothing is buried in these areas (between horizontal distances of 0 and 0.1 m, and 0.33

m and 0.4m). These artifacts might still be due to reflection from the sides and need to be investigated.

Figure 4.13 shows a B-mode image where the targets were two small plates buried at the same depth of 12 cm. The plates were a distance of around 7 cm from each other. The two plates can be seen on the reconstructed image. But the artifacts are present on the left side with a high intensity. One plate is seen between horizontal distances of 0.1 m and 0.2 m and the other between horizontal distances of 0.26 and 0.36 m. The targets also seem to create two shapes instead of one. This is probably due to the two cycles of the transmitted pulse. Also, the right plate creates a higher amplitude echo than the left plate. Because the plates were buried at the same depths, the stronger echo of the second plate is probably due to a better contact with the sand of the devices when acquiring the data for the right side of the scan. This image shows that the lateral resolution permits at least to resolve targets located at a distance of 7 cm from each other.

4.2.3 Delay-and-sum images

For all the delay-and-sum images presented in this section, the transmitted pulse was a 2-kHz, two-cycle sine wave. The peak-to-peak voltage going into the MST was 300 V. Here also, 32 signals were averaged for each receiving position with a PRF of 10 Hz. The step size was equal to 1 cm. On receive, a five-element line array was used. The distance between two consecutive elements was 1 cm and the distance between MST and the first receiving position was 23 cm. This scan geometry is shown in Figure 4.14.

Figure 4.15 shows a reconstructed image of the same target as in Figure 4.12: four plates. This image was obtained using delay-and-sum beamforming with a single depth of focus of 0.1 m. This depth was chosen because it is the depth at which the targets were buried. Figure 4.16 shows the reconstruction from the same data but with the use of dynamic focusing. Dynamic focusing was used with 20 discrete depths of focus on a 1-m range; therefore, signals were focused every 5 cm. On both figures the targets are seen. But In Figure 4.16 more artifacts are present, particularly on the right side of the image. This is a consequence of the use of DF with experimental data where noise is also present. DF also helps bring up noise at every depth. Figure 4.15 is focused on the target only; therefore, most of the image is out of focus. Basically, the noise is out of phase at almost every depth and therefore has less impact on the reconstructed image.

Figures 4.12 and 4.15 were obtained using the same target configuration.

One can easily see that the use of the array improves the axial resolution. The pattern generated by the targets in Figure 4.12 was 20 cm wide in the range direction; it is now only around 10 cm in Figure 4.15. However, the lateral resolution did not change; the pattern is around 20 cm wide in the horizontal direction in both figures.

Figures 4.17 and 4.18 were obtained with a single plate buried at a depth of 10 cm. The plate was buried so that its longest direction was perpendicular to the direction of the scan. Figure 4.17 was reconstructed using delay-and-sum beamforming with a single depth of focus of 0.1 m (depth of the target). Figure 4.18 was reconstructed from the same data but with the use of DF with 20 depths of focus regularly spread on a 1-m range.

Figures 4.17 and 4.18 show very similar images. The target can be seen, but many artifacts are present on the sides and below the targets. The sides artifacts can also be interpreted as reflections from the walls. The big pattern present below the target at a depth of around 0.22 m can be due to multiple reflections from the small plate. The only difference between Figures 4.17 and 4.18 is in the amplitude levels of the patterns present on the images. Figure 4.18, reconstructed with DF shows, higher energy levels almost everywhere. For example, in the pattern generated by the target in the middle of the figures and at a depth of 0.12 m, the amplitude is around 6 dB higher in Figure 4.18 than in Figure 4.17. This last fact is also true for most of the artifacts present in both figures. This is a consequence of DF, which helps to concentrate the energy at every depth by making signals arrive in phase. Higher amplitudes in the patterns present in the image when DF is used were also seen in a simulation image (Figure 4.5).

The study of the experimental images has shown the presence of side artifacts in almost all pictures. The cause of these artifacts needs to be investigated. The artifacts limit the ability to take full advantage of the experimental system. Therefore, a solution must be found to reduce their presence.

4.3 Direct Wave Issue

4.3.1 B-mode images in sandbox without target

The previous scans (Sections 4.2.2 and 4.2.3) showed artifacts in the images. Since the artifacts were mostly present on the sides of the pictures, we thought that they were due to reflections from the sidewalls of the box.

Therefore, running scans without targets in the sandbox was done to evaluate artifacts as a function of the distance between transducers and the sides of the box.

These scans were acquired along one direction, with the segment MST-Terr perpendicular to this direction. The step size was 5 cm, so that each scan did not take more than 15 min. The results are shown in Figures 4.19-4.23.

The only difference between these five scans is the center-to-center distance between MST and Terr, which increases from 13 cm in Figure 4.19 to 30 cm in Figure 4.23.

These figures show a parasite signal constant along the whole scan, which means that it is not generated by the sides. The beginning of the parasite signal in time is shown to be a linearly increasing function of the center-to-center distance. Figure 4.24 shows this last fact. In this figure, the time represents the beginning of the parasite signal and the distance is the distance between MST and Terr. The solid line is formed with five points based on the average values of the beginning in time of the DW from Figures 4.19-4.23. The dashed line is the linear fit of these five points. The linear fit has a slope of 149.6 m/s The fact that the solid curve is very close to a straight line tends to confirm that this parasite signal is a direct wave propagating directly from MST to Terr.

Using Figure 4.24, the speed of the direct wave is therefore around 150 m/s. This value is smaller than the speed of the fast wave in sand, which is around 200 m/s.

4.3.2 Received direct wave signal and imaging issues

A study of the direct wave signal is necessary to determine the consequences in terms of imaging. We hence used some signals from the previous scans and looked at them more carefully to have an idea of how the direct wave signal would affect imaging.

The top curve of Figure 4.25 shows one received signal when the center-to-center distance was 16 cm (used to build Figure 4.20), and the bottom of Figure 4.25 shows its spectrum. Figure 4.25 clearly shows that the direct wave is about four cycles even though the source was driven by an electrical signal composed of two cycles. A source electrical signal composed of one cycle also yielded a four-cycle receive signal. The spectrum shows that most of the energy is still around 2 kHz, which shows that the direct wave also has a frequency of 2 kHz. Hence the direct-wave wavelength would be around

150 m/s / 2000 Hz=7.5 cm.

The existence of a four-cycle receive signal plus the time delay, due to the propagation of the direct wave between MST and Terr, creates a dead zone of around 30 cm in depth, where imaging an object would be very difficult.

The fact that the direct wave also has a frequency of 2 kHz eliminates the possibility of filtering in the frequency domain to segment the direct wave from the signals originating at greater depths where targets are located.

4.4 Solutions Tried to Mitigate the Direct Wave

4.4.1 Sound absorbing material

The origin of the surface wave is probably related to the coupling between the transducers and the sand. Hence one can think that using some kind of material in between the transducers and sand might yield another kind of coupling and might therefore mitigate the direct wave. This is why we used different kinds of sound absorbing material.

We used a piece of neoprene of 6 mm in thickness and two kinds of sound absorbing material (SOAB). They are known to have an impedance comparable to that of water. The SOAB, made by Goodrich & Co., was of a silver color and 2.5 cm. The other material, called Wallgone (Consumer Usage Laboratories, Inc.) was red and about 1 cm thick. Figure 4.26 shows a picture of the three materials.

The experiment consisted in putting the piece of material on the top of the sand box. We then acquired B-mode data as described in Section 4.3.1.

Figure 4.27 shows a B-mode image made with the silver SOAB and a small plate buried 22 cm deep as target. Figure 4.28 shows one of the received signals from over the plate and its spectrum. Figure 4.27 shows that the direct wave is still present because we can see a parasite signal present along the whole scan. Figure 4.28 shows that the DW seems now to be composed of around six cycles and starts earlier than without the SOAB. It starts at a time of 0.2 ms in Figure 4.28 compared to 0.8 ms in Figure 4.25. This last fact is simply due to the higher speed of the direct wave in the SOAB than in the sand. A study demonstrated a speed of propagation of around 800 m/s.

However, in Figure 4.27 the target seems to be visible, but its range is off: it is visible at a depth of 0.3 m but is buried at a depth of 0.22 m. This is not due to the layer of SOAB. Because the speed of propagation in the

SOAB is around 1500 m/s, the time necessary to go through the layer (2.5 cm thick) is too small to result in an error of 8 cm.

Actually, maybe the object is seen in the picture at its correct depth but with a low amplitude instead. This can be a consequence of interferences between the direct wave signal and the signal reflected from the target.

The trial with SOAB has shown that it was not an acceptable solution because the direct wave is still present, and even if it starts earlier (0.2 ms compared to 0.8 ms) it still ends too late because it is apparently composed of more cycles (six cycles compared to four cycles).

4.4.2 Water layer

The previous soil imaging study [14] using a water layer did not have a direct wave propagation phenomenon. We thought that reproducing the conditions of the previous experiments–that is, using a water layer– might get rid of the direct wave.

We put a small plastic pool on the top of the sandbox that we filled with 2 cm of water. Then three configurations were tried. In the first configuration Terr is touching the bottom of the pool and the transmitter is in contact with the water but not with the bottom of the pool. In the second configuration both transducers are touching the bottom of the pool. Finally, in the third configuration both transducers are in contact with the water but not with the bottom of the pool. For these three experiments, the PST was used because putting MST into the water will damage it. The first and third experiments did not yield any noticeable receive signal. This is probably due to the PST not having a good coupling with water. Terr was also the receiver in the previous soil imaging study [14]. The second led to very similar receive signals as without the pool. Particularly, the direct wave was still present. This result is due to the fact that when Terr and PST are touching the bottom of the pool, the presence of the water layer does not change their properties in terms of energy transmission in the sand.

These results demonstrate that the water does not constitute an acceptable solution.

4.4.3 Destructive summation

This direct wave (DW) has a frequency of 2 kHz, and its speed was measured to be around 150 m/s (slower than the wave traveling in the sand whose speed is around 200 m/s); thus its wavelength is $\lambda = 7.5$ cm. The idea was hence to receive signals containing a delayed version of the DW such that their summation might result in the cancellation of the DW.

Figure 4.29 demonstrates the fact that summing the correctly phased versions of the DW might result in its cancellation. This figure shows the summation of 16, four-cycle 2-kHz sine waves regularly spread over one wavelength. The value four has been chosen for the number of cycles to be the same as what is experimentally seen. This figure is therefore a crude simulation of the summation of 16 direct wave signals regularly spread over one wavelength. Figure 4.29 shows that, after summation, only the first half of the first cycle and the last half of the last cycle are still visible. It is of course the ideal case, where all the cycles have the same amplitude, and where the value of the wavelength is the same. In that simulation the amplitude of the waves was assumed to be one.

However, Figure 4.29 assumes that the waves have a constant amplitude, which is not the case because, as the receiver moves away from the source, the direct wave has a longer path to travel and hence attenuates more. So Figure 4.29 assumes either no attenuation or a perfect compensation of the attenuation.

Figure 4.30 shows the case where attenuation is included but not compensated. The attenuation chosen was 1.2 dB/cm. It comes from the measured value of 0.6 dB/kHz/cm multiplied by the frequency used of 2 kHz. This tends to show that to achieve good cancellation one needs to compensate for the attenuation in some way. Note that in Figure 4.30 the maximum amplitude is 0.03. The difference in the maximum amplitudes between Figures 4.29 and 4.30 is the due to the attenuation having been applied to sine waves of amplitude 1 on Figure 4.30.

Based on the idea of summing sine waves spread out over a wavelength, a linear scan was run. The scan consisted of 50 steps: 50 cm long with a step size of 1 cm. On receive an eight-element linear array was used. The first element was at a distance of 20 cm from the source and the last one at a distance of 35 cm. This means that the receiver covered a distance of two wavelengths of the direct wave, because for the DW $\lambda = 7.5$ cm. Figure 4.31 describes this geometry seen from the top of the sand box. The source pulse was a two-cycle, 2-kHz sine wave, and a small plate was buried 18 cm deep. This plate has for dimensions 1.2 cm x 7.5 cm x 60 cm. It was buried with the longest side perpendicular to the scanning direction.

Figure 4.32 shows the reconstructed images without DF at four different depths of focus. All four images are reconstructed at the same scale. The top-left image is focused at a depth of zero, the top-right at 9 cm, the bottom-left at 18 cm (depth of the target), and the last one at infinity (that means no delay, the signals were directly summed).

Figure 4.33 shows the picture reconstructed using dynamic focusing from the same data as in Figure 4.32. The signals were focused at 20 regularly spaced depths so that all the picture is in focus. Since the image is reconstructed up to a depth of 50 cm, it makes the focus depths to be 2.5 cm apart.

In the top left image of Figure 4.32 the direct wave has almost totally disappeared and the target can be seen. The target seems to be 15 dB higher in amplitude than the DW. However, on the three others images of Figure 4.32 the DW is present but the target can be seen as an object of low amplitude. The target is this time around 15 dB lower than the surrounding structures on the top-right and bottom-left images and 10 dB lower in the bottom right picture. Figure 4.33 shows the same phenomenon as the top right image of Figure 4.32. The target is seen with an amplitude 15 dB lower than the DW. The fact that the results provided using DF (Figure 4.33) are similar to the the top right image of Figure 4.32 is logical because the top right image of Figure 4.32 is focused at the depth of the target.

The good point of the results shown by Figures 4.32 and 4.33 is that the target can be seen in all of them. But the results are surprising. We did not expect the direct wave to cancel out and to bring up the target with a focus at a depth of 0. Actually, the scan had been designed so that the DW should cancel out when there are no delays; this case would correspond to the bottom right image of Figure 4.32, but in this image the DW is still clearly present. This phenomenon might be a consequence of a slight error in the speed of propagation of the DW, which will lead to an error in the wavelength. An error in the wavelength could then destroy the scheme of destructive interferences that we set up and lead to an amplification of the DW instead of its cancellation. Another reason might be the fact that the attenuation of the DW is not compensated for, and thus the cancellation would not be total even if we were summing correctly phase-shifted sine waves as shown in Figure 4.30.

The idea of cancelling out the DW by summing regularly delayed versions is interesting but led to surprising results, where the DW should have been canceled out and the target should appear. Actual results show a DW still present and a target with a lower amplitude. An error in the speed of propagation of the DW might explain this phenomenon.

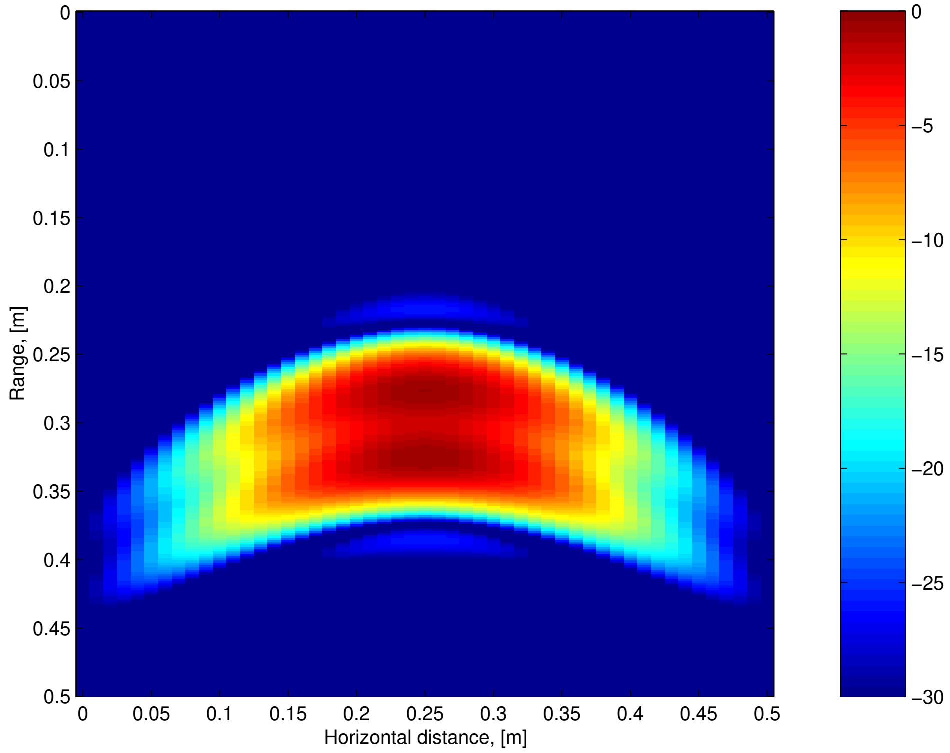

Figure 4.1: Pulse-echo simulation with a single point target reflector at a depth of 0.25 m. Reconstructed without DF and TGC.

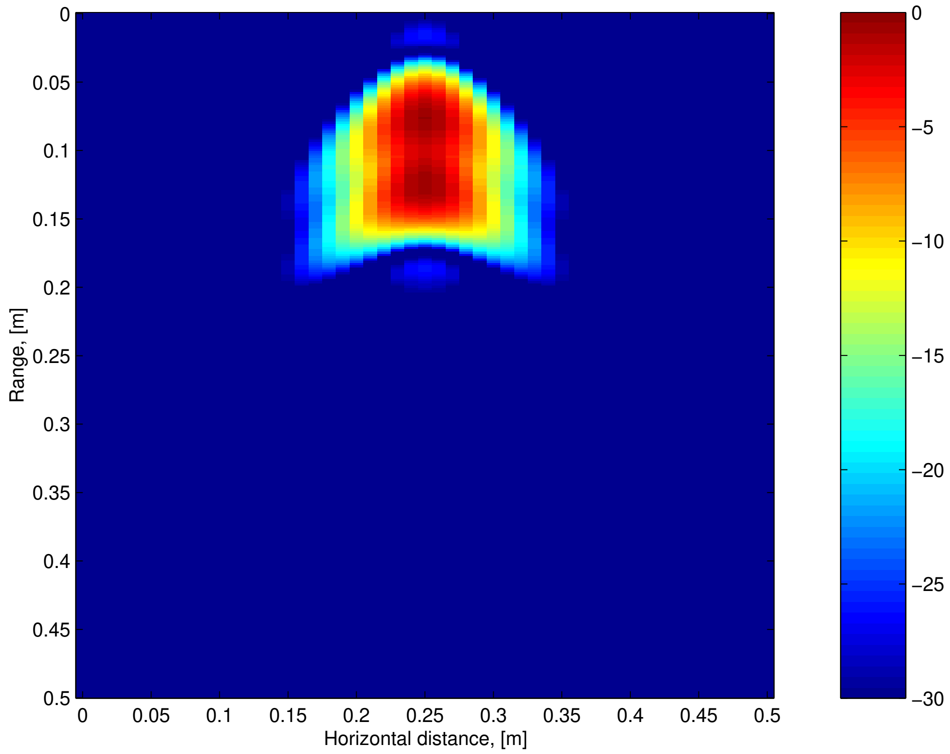

Figure 4.2: Five point targets reconstructed from simulated data, single receiving element, without TGC. Targets located at depths 0.05 m, 0.15 m, 0.25 m, 0.35 m, and 0.45 m.

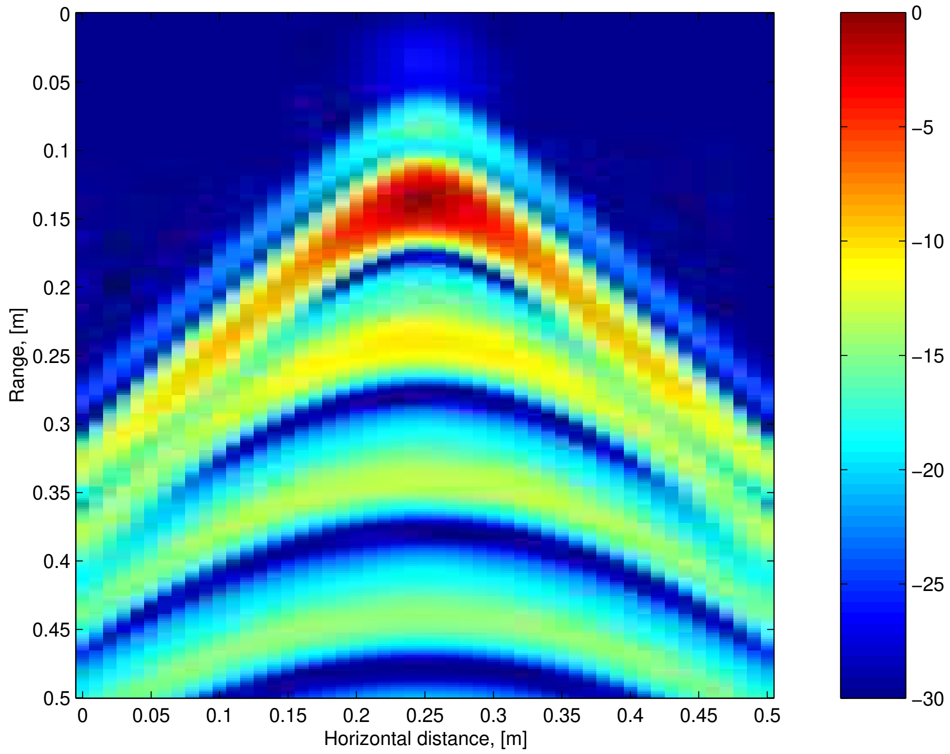

Figure 4.3: Five point targets reconstructed from simulated data, single receiving element, with TGC. Targets located at depths 0.05 m, 0.15 m, 0.25 m, 0.35 m, and 0.45 m.

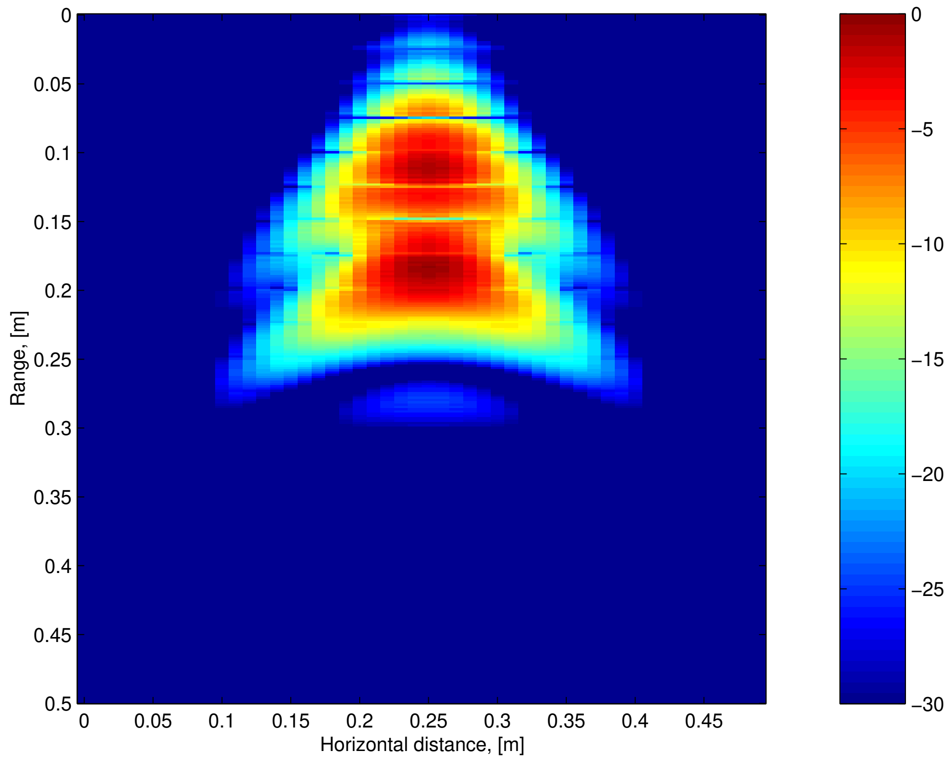

Figure 4.4: Five point targets reconstructed from simulated data, eight-element line array on receive, without TGC. Targets located at depths 0.05 m, 0.15 m, 0.25 m, 0.35 m, and 0.45 m. The array was along the direction of scanning, and the elements were 1.8 cm apart. Dynamic focusing was used with 20 different depths of focus. DF was accomplished without smoothing.

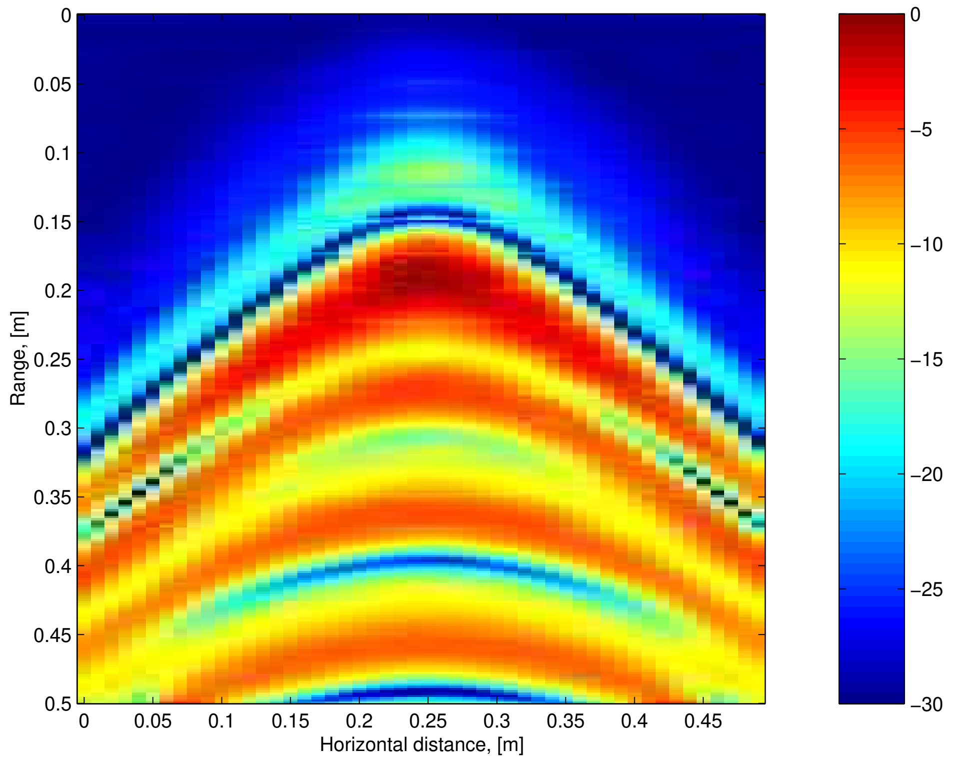

Figure 4.5: Five point targets reconstructed from simulated data, eight-element line array on receive, with TGC. Targets located at depths 0.05 m, 0.15 m, 0.25 m, 0.35 m, and 0.45 m. The array was along the direction of scanning, and the elements were 1.8 cm apart. Dynamic focusing was used with 20 different depths of focus. DF was accomplished without smoothing.

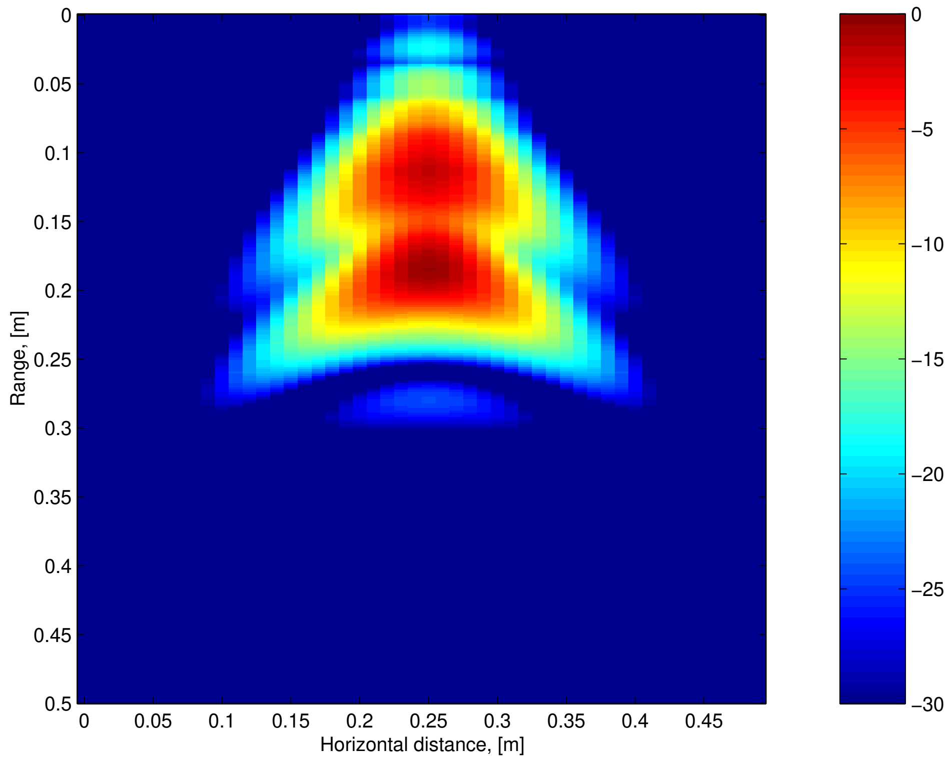

Figure 4.6: Five point targets reconstructed from simulated data, eight-element line array on receive, without TGC. Targets located at depths 0.05 m, 0.15 m, 0.25 m, 0.35 m, and 0.45 m. The array was along the direction of scanning, and the elements were 1.8 cm apart. Dynamic focusing was used with 20 different depths of focus. DF was accomplished with smoothing.

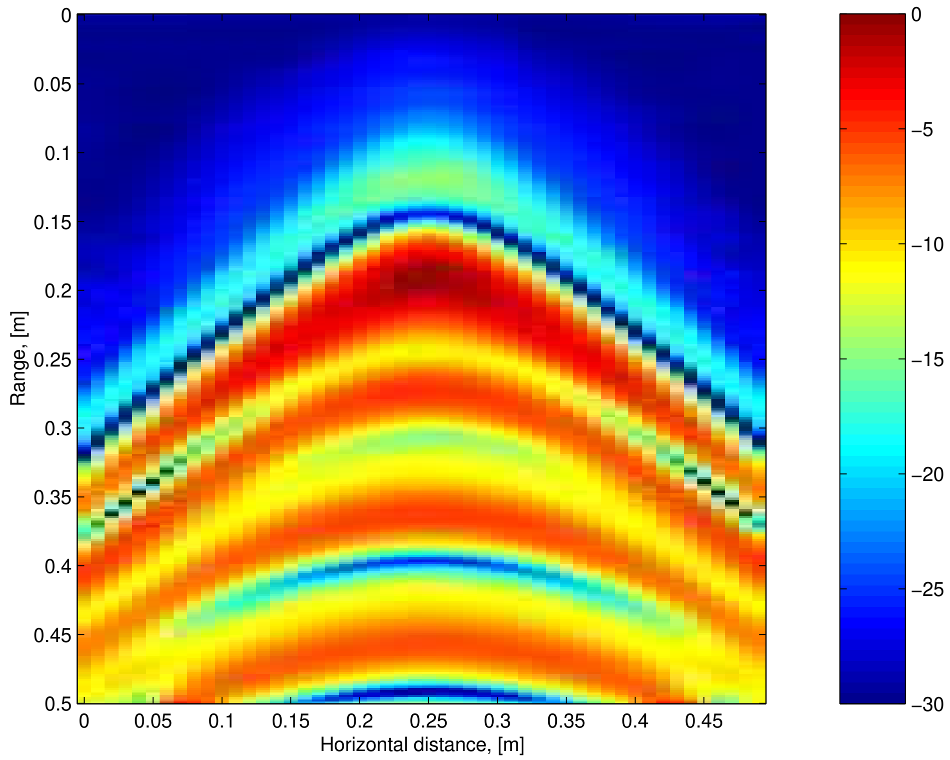

Figure 4.7: Five point targets reconstructed from simulated data, eight-element line array on receive, with TGC. Targets located at depths 0.05 m, 0.15 m, 0.25 m, 0.35 m, and 0.45 m. The array was along the direction of scanning, and the elements were 1.8 cm apart. Dynamic focusing was used with 20 different depths of focus. DF was accomplished with smoothing.

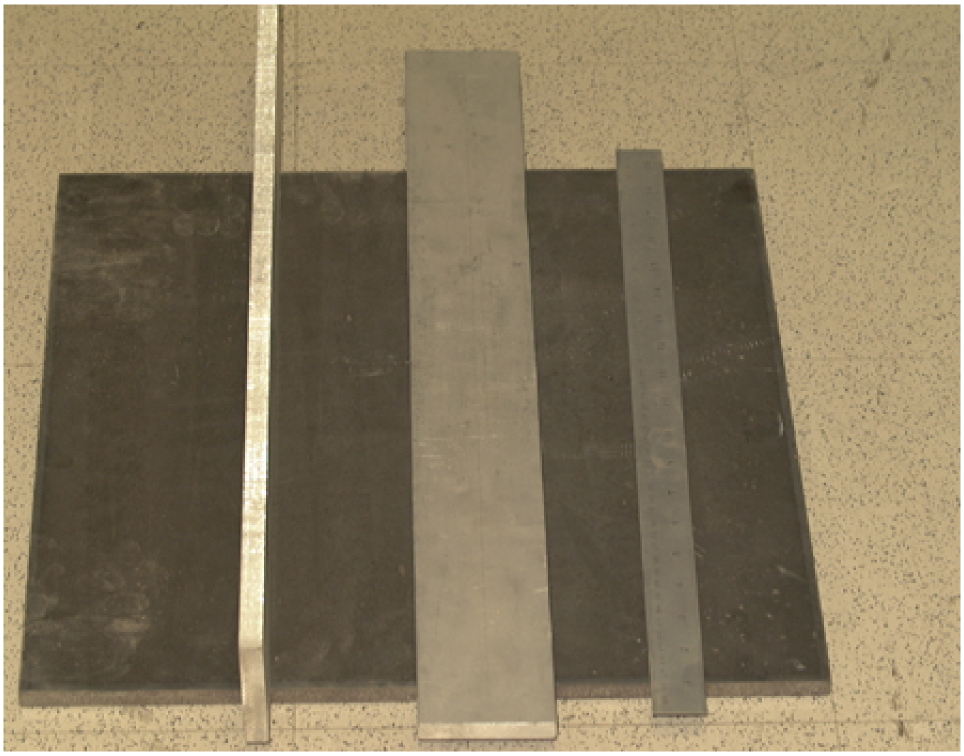

Figure 4.8: Pictures showing the targets used in the experiments. The big steel plate and two small plates. The ruler at the right is 50 cm long and 3 cm wide.

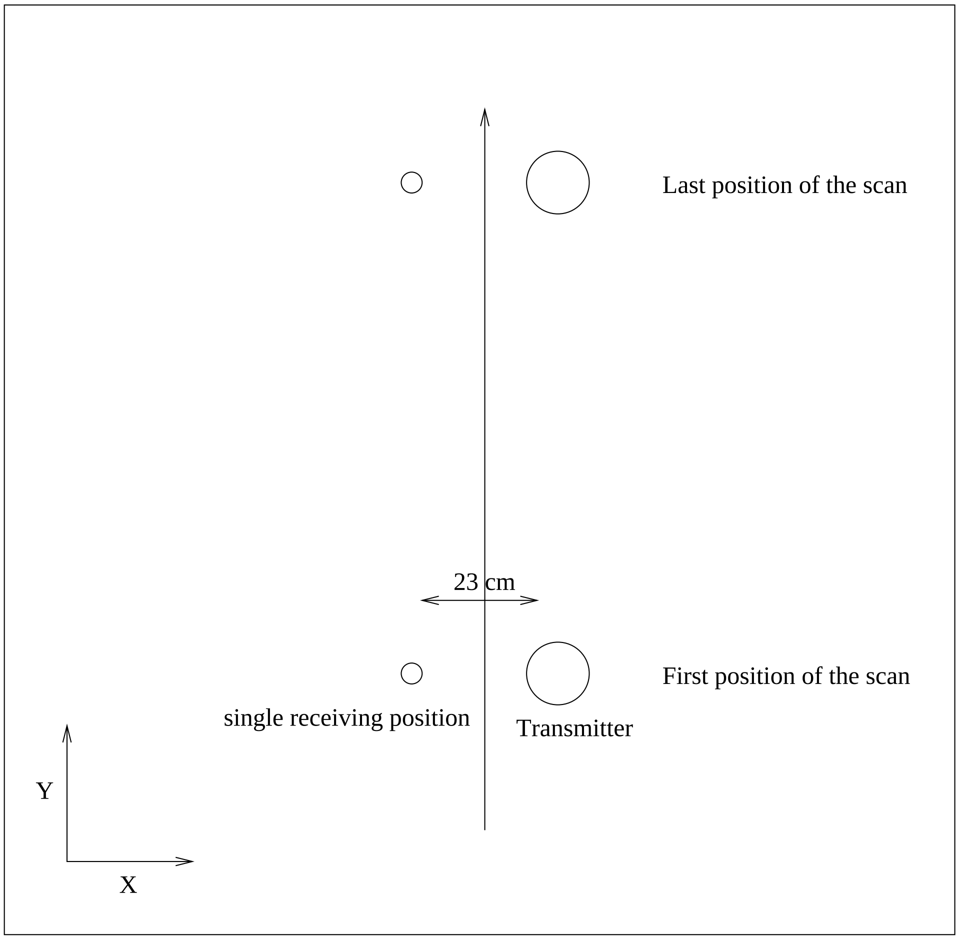

Figure 4.9: Scan geometry used to reconstruct B-mode images.

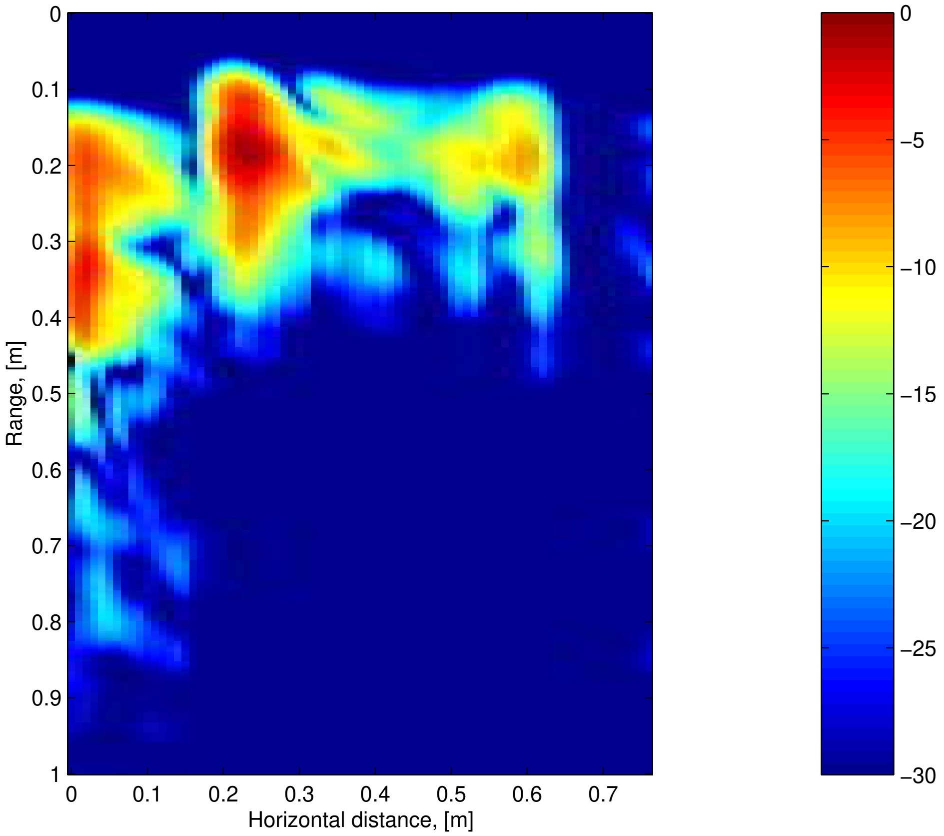

Figure 4.10: B-mode image. MST is transmitter, Terr is receiver, and the big steel plate is buried 10 cm deep as target. Transmitted pulse: 2 kHz, two cycles.

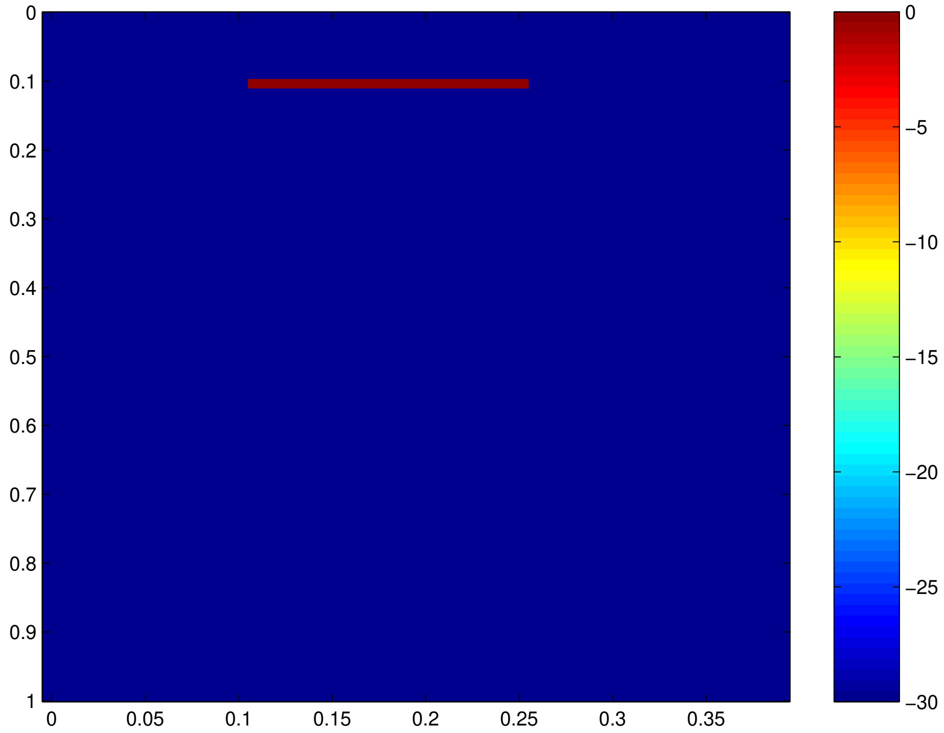

Figure 4.11: Geometry of the four plates stacked together as target.

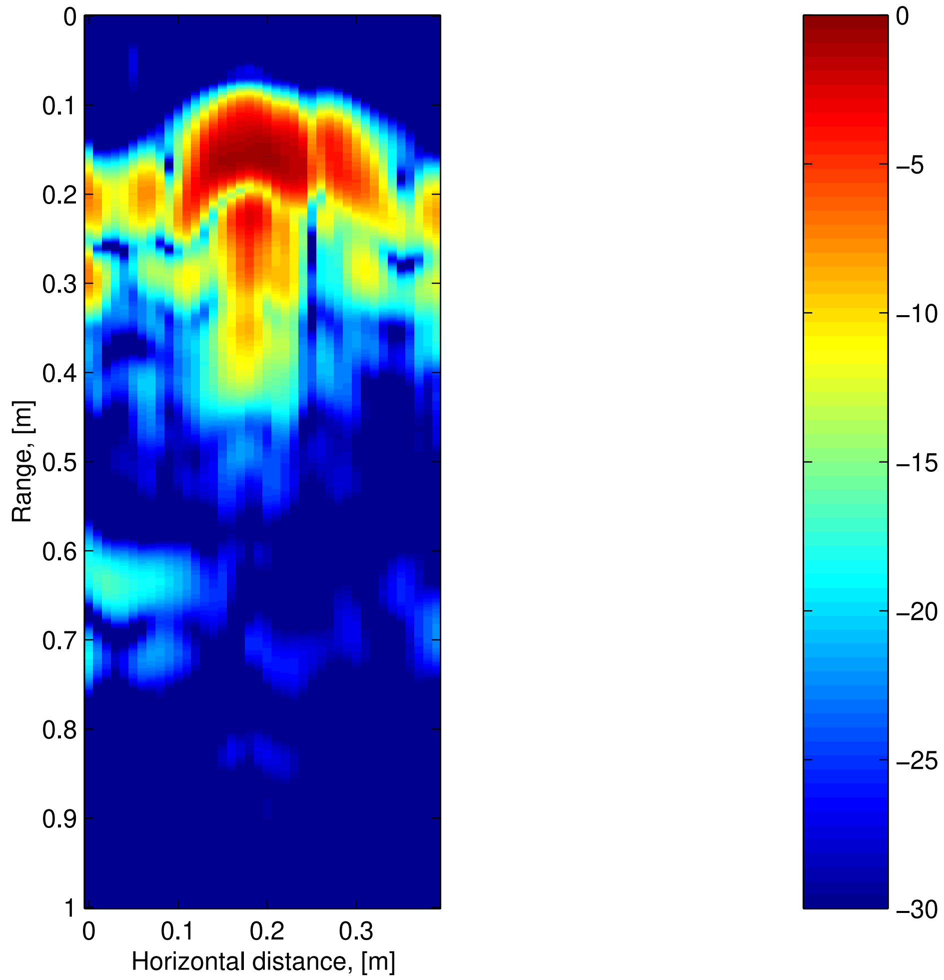

Figure 4.12: B-mode image. MST is transmitter, Terr is receiver, and four plates as target (Figure 4.11). Transmitted pulse: 2 kHz, two cycles.

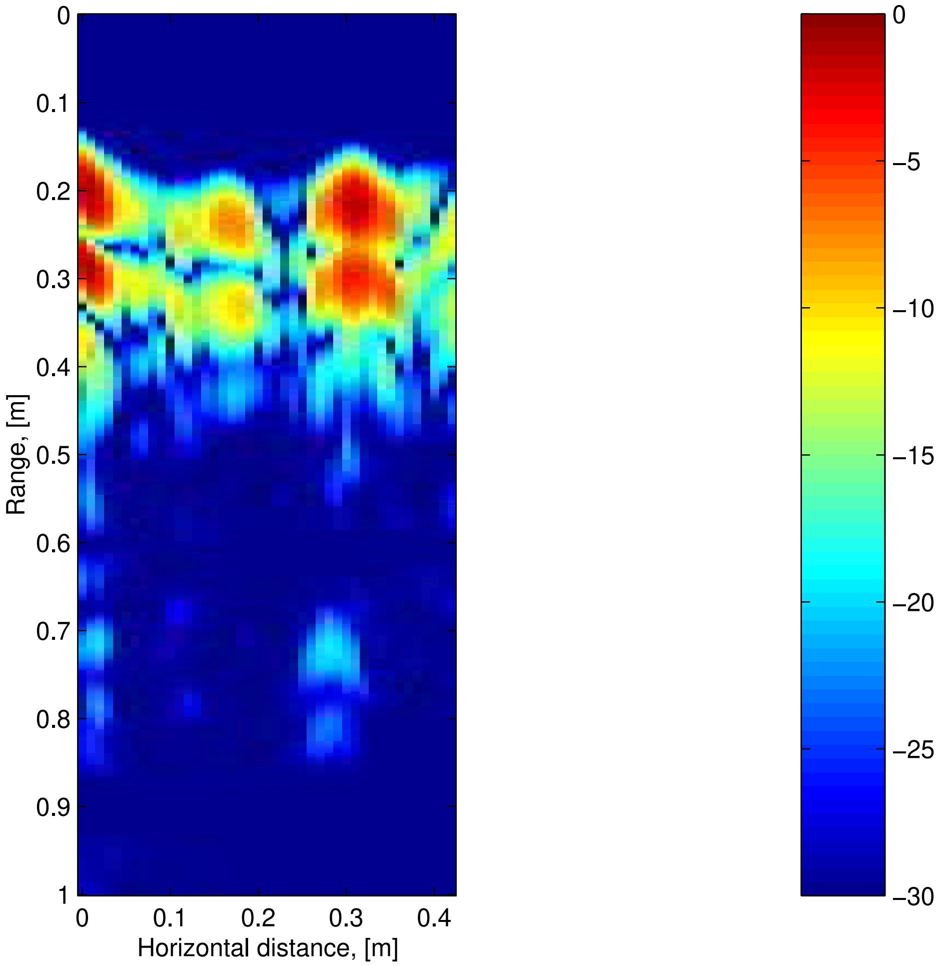

Figure 4.13: B-mode image. MST is transmitter, Terr is receiver, and two plates as target buried 12 cm apart at a depth of 17 cm. Transmitted pulse: 2 kHz, two cycles.

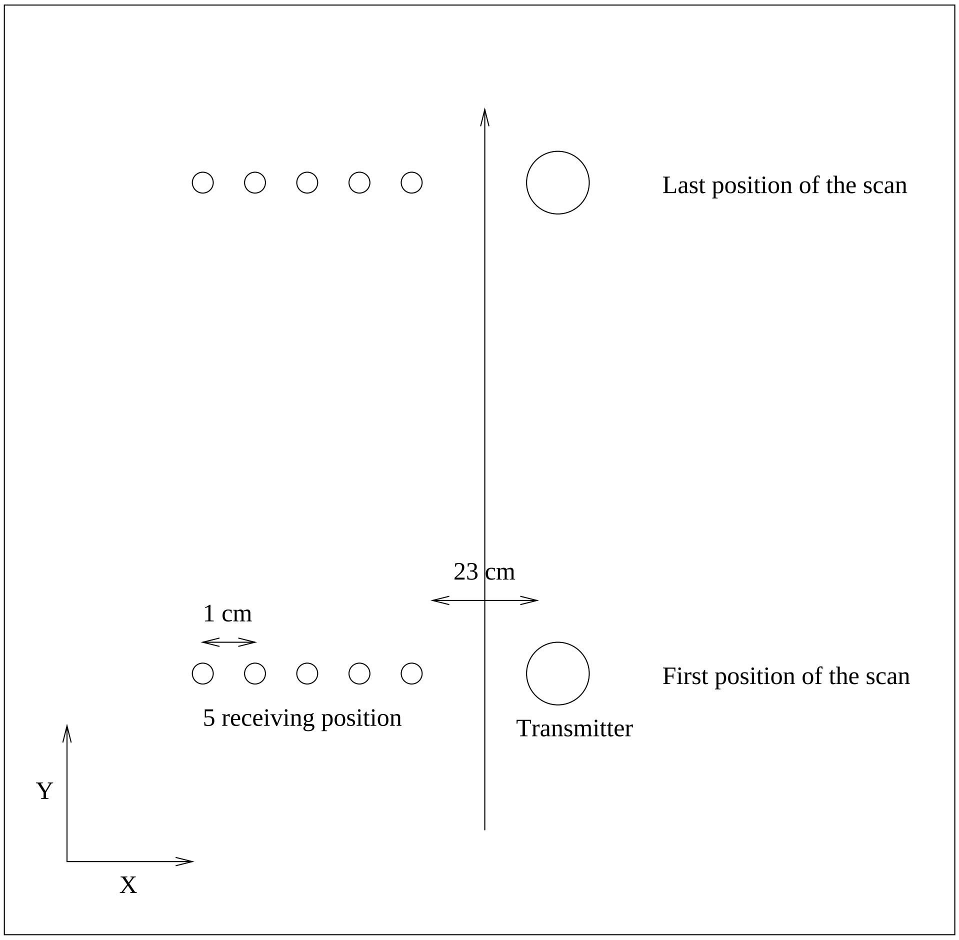

Figure 4.14: Scan geometry used to reconstruct delay-and-sum images. On receive a five-element linear array is used.

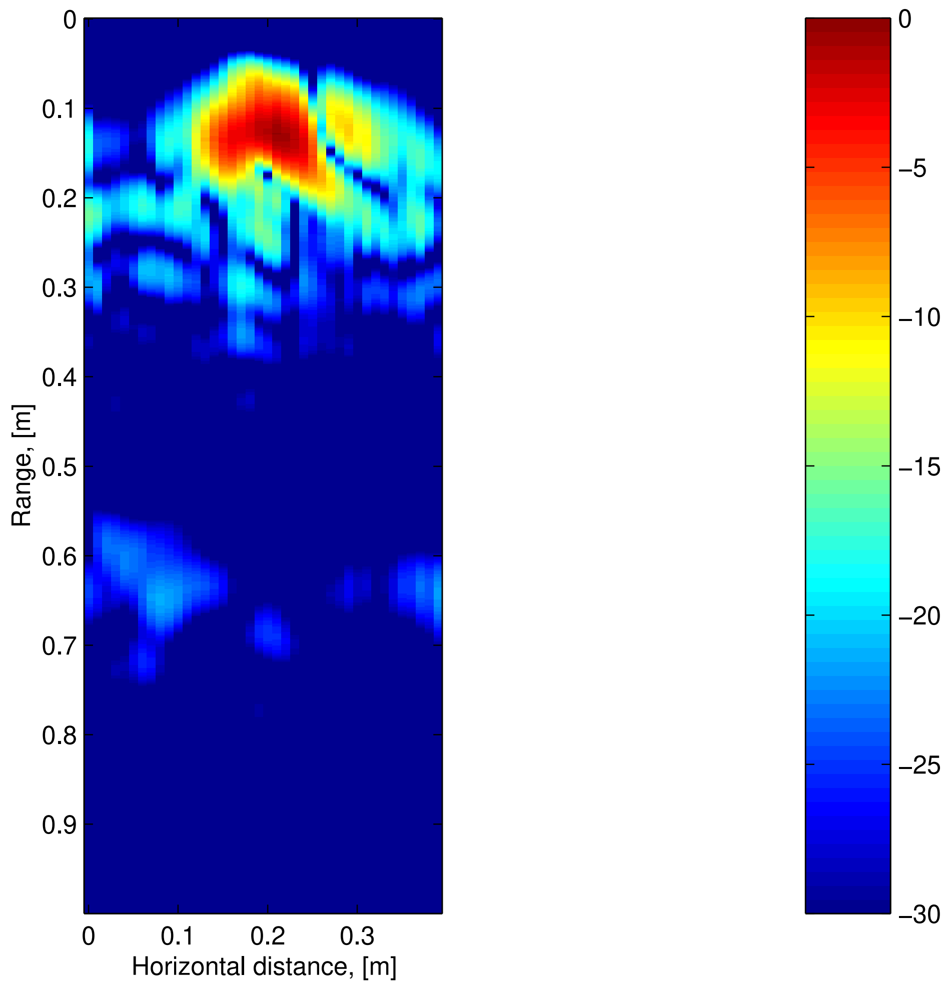

Figure 4.15: Delay-and-sum image. MST is transmitter, Terr is receiver, and four plates as target (Figure 4.11). 0n receive a five-element linear array is used. Transmitted pulse: 2 kHz, two cycles. Image reconstructed using a single depth of focus of 0.1 m.

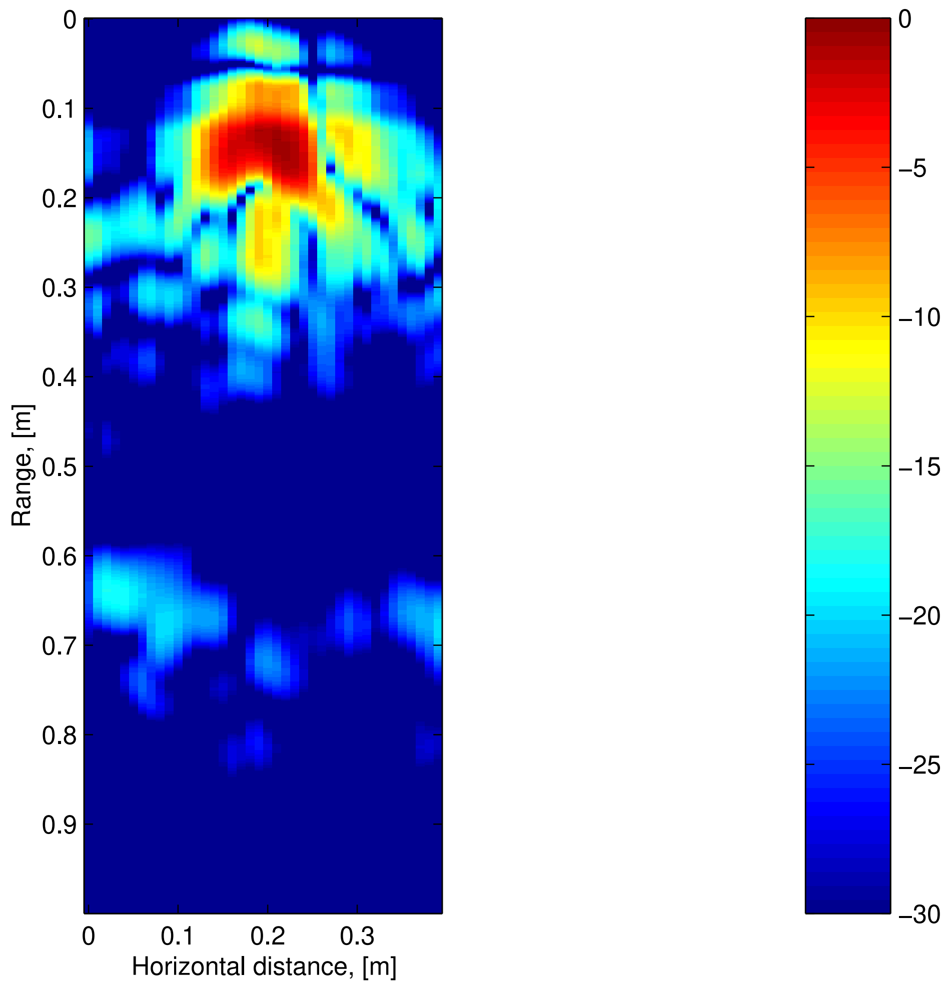

Figure 4.16: Delay-and-sum image. MST is transmitter, Terr is receiver, and four plates as target (Figure 4.11). 0n receive a five-element linear array is used. Transmitted pulse: 2 kHz, two cycles. Image reconstructed using 20 depths of focus on a 1-m range.

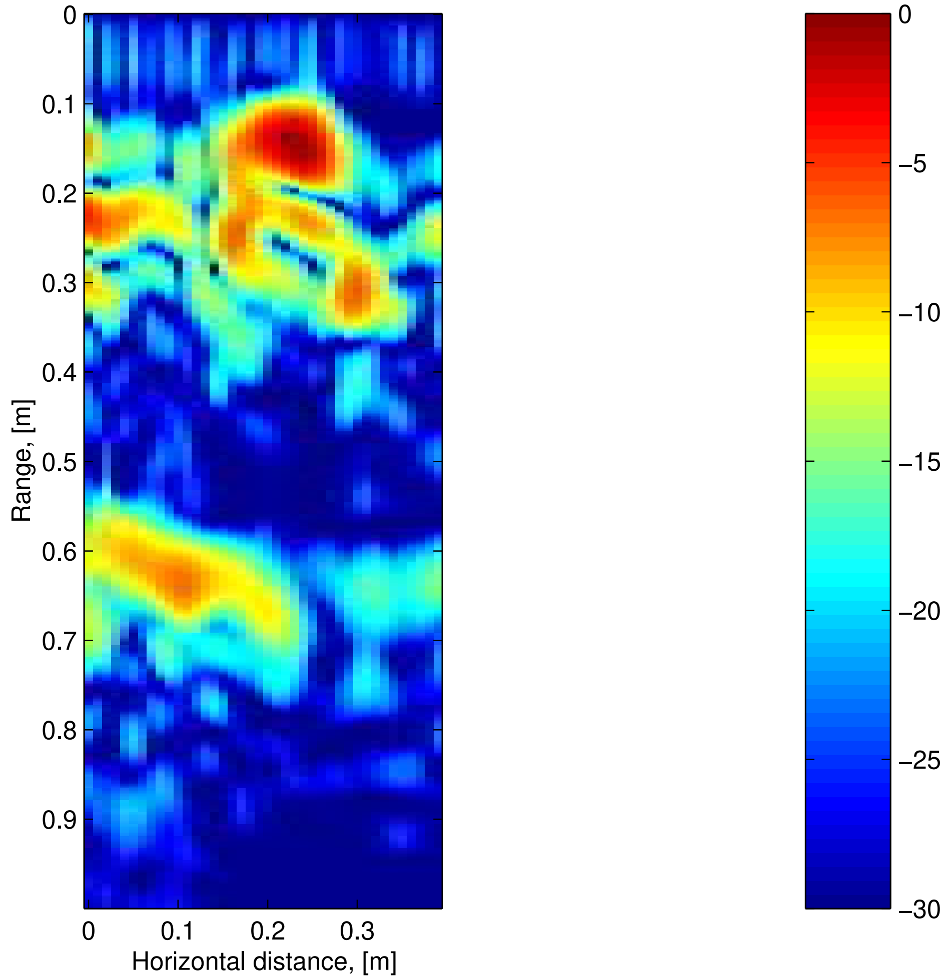

Figure 4.17: Delay-and-sum image. MST is transmitter, Terr is receiver, and one plate as target buried 10 cm deep. 0n receive a five-element linear array is used. Transmitted pulse: 2 kHz, two cycles. Image reconstructed using a single depth of focus of 0.1 m.

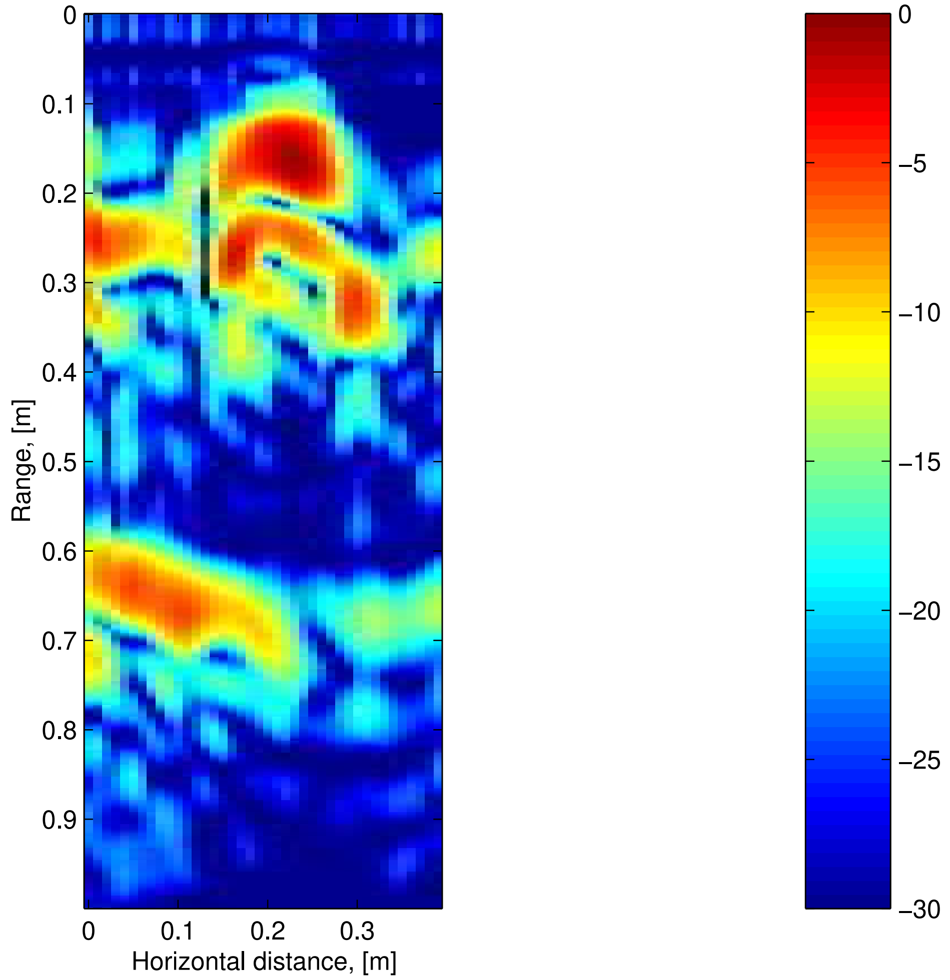

Figure 4.18: Delay-and-sum image. MST is transmitter, Terr is receiver, and one plate as target buried 10 cm deep. 0n receive a five-element linear array is used. Transmitted pulse: 2 kHz, two cycles. Image reconstructed using 20 depths of focus on a 1-m range.

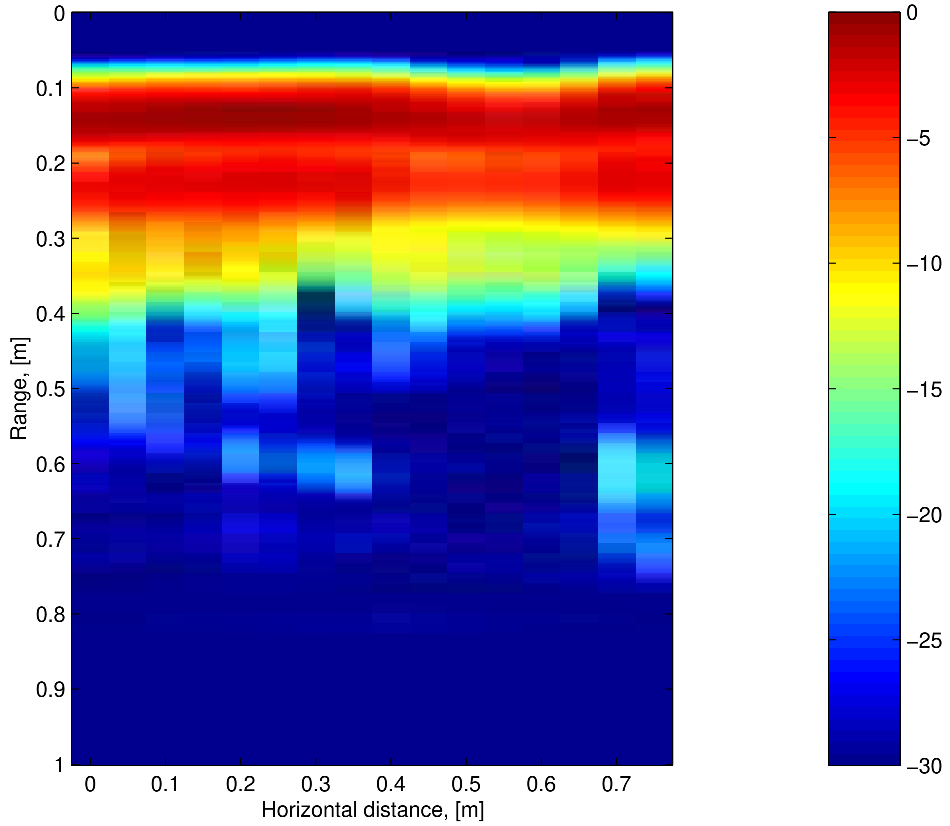

Figure 4.19: Linear scan across the sand surface without targets. MST is transmitter and Terr is receiver. The MST-Terr distance is 13 cm, and the source electrical signal is 2 kHz, two cycles.

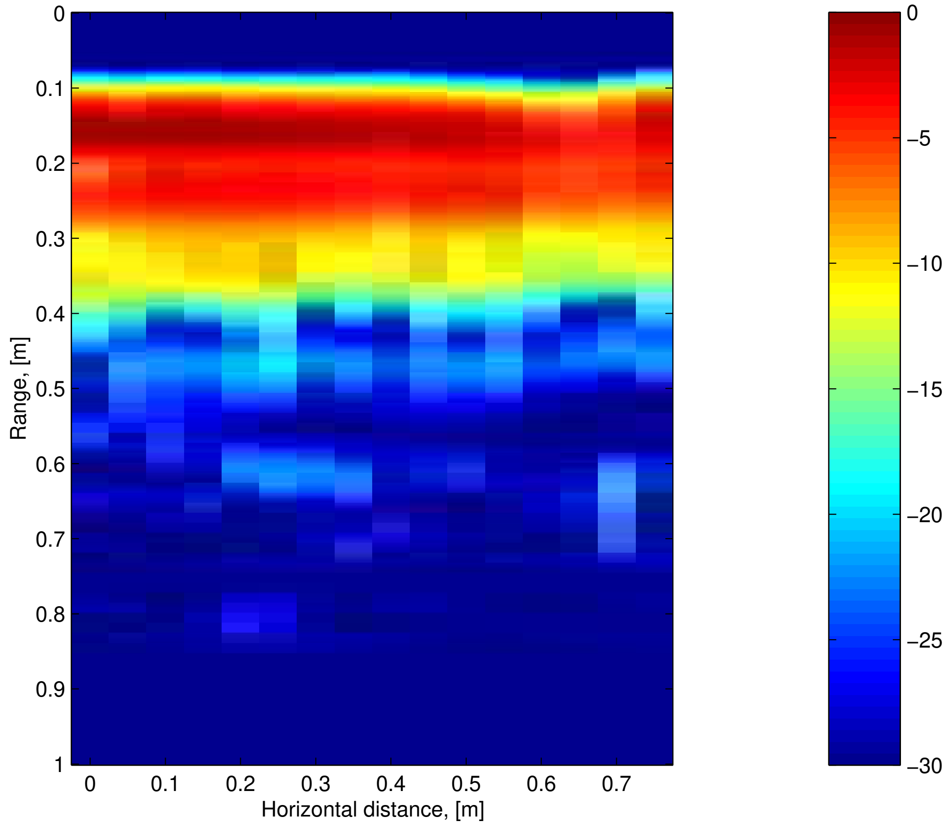

Figure 4.20: Linear scan across the sand surface without targets. MST is transmitter and Terr is receiver. The MST-Terr distance is 16 cm, and the source electrical signal is 2 kHz, two cycles.

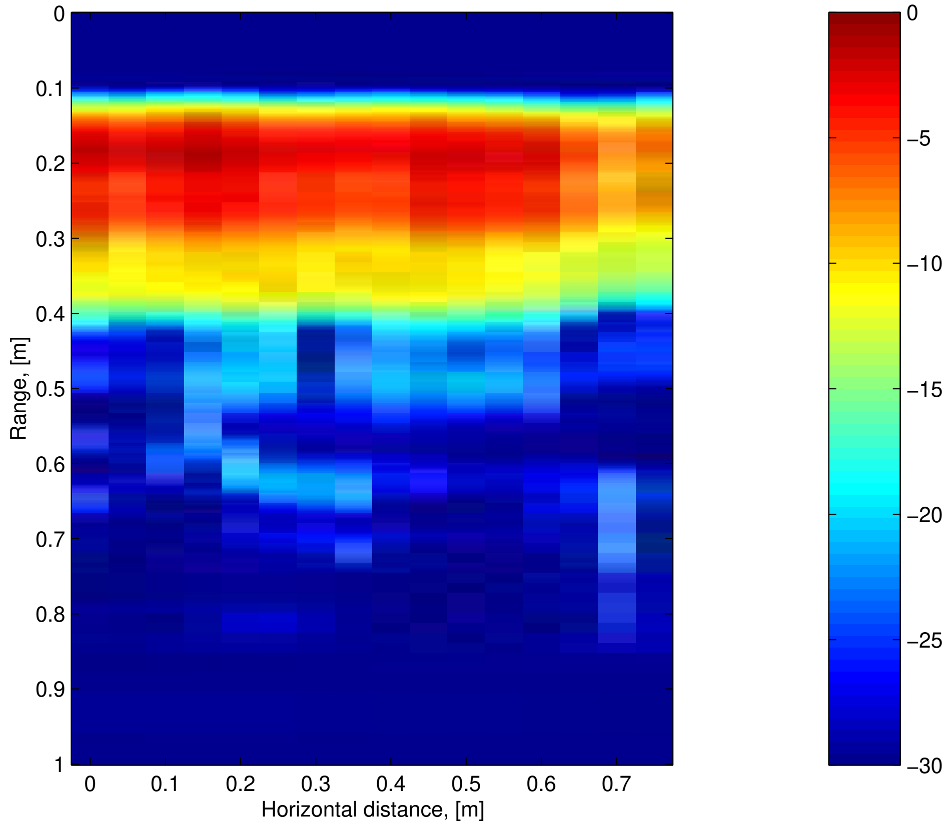

Figure 4.21: Linear scan across the sand surface without targets. MST is transmitter and Terr is receiver. The MST-Terr distance is 20 cm, and the source electrical signal is 2 kHz, two cycles.

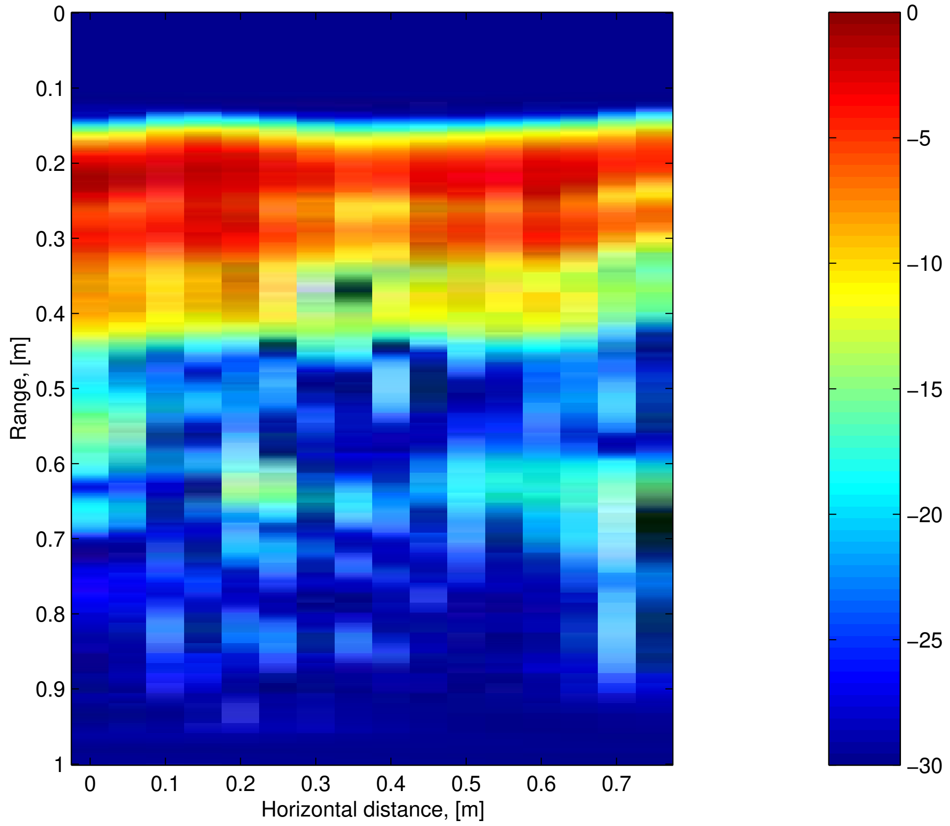

Figure 4.22: Linear scan across the sand surface without targets. MST is transmitter and Terr is receiver. The MST-Terr distance is 25 cm, and the source electrical signal is 2 kHz, two cycles.

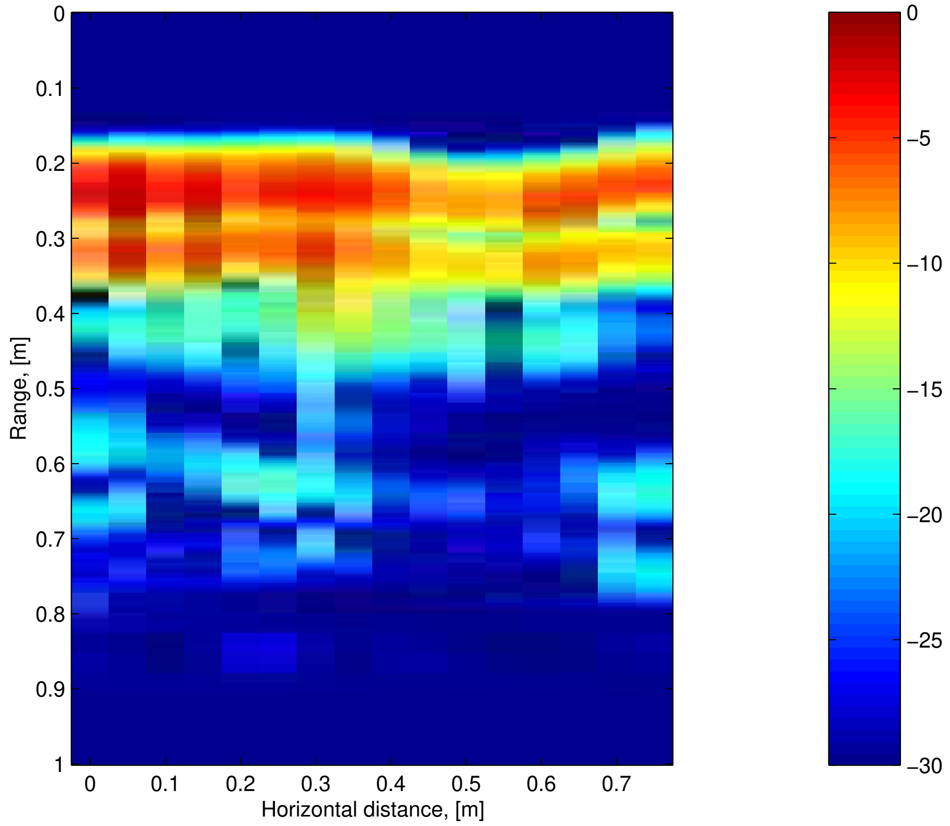

Figure 4.23: Linear scan across the sand surface without targets. MST is transmitter and Terr is receiver. The MST-Terr distance is 30 cm, and the source electrical signal is 2 kHz, two cycles.

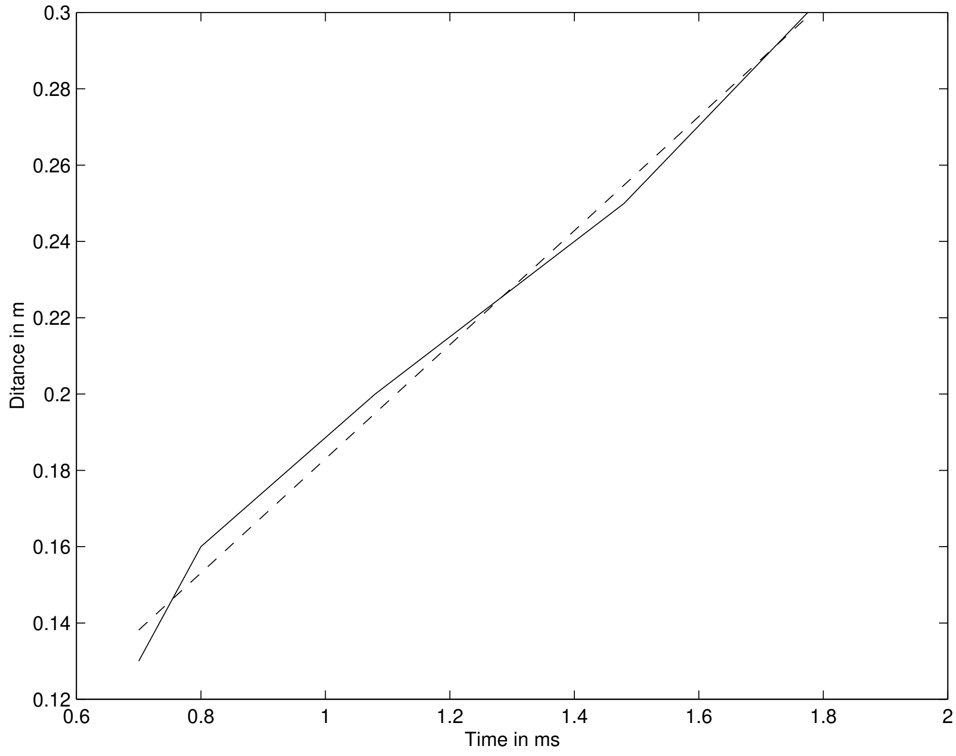

Figure 4.24: Figure showing that the beginning in time of the parasite signal from Figures 4.19–4.23 is linear with the MST-Terr distance. Solid is the curve based on five points obtained from the five figures. Dashed is the linear interpolation, the slope is 149.6 m/s.

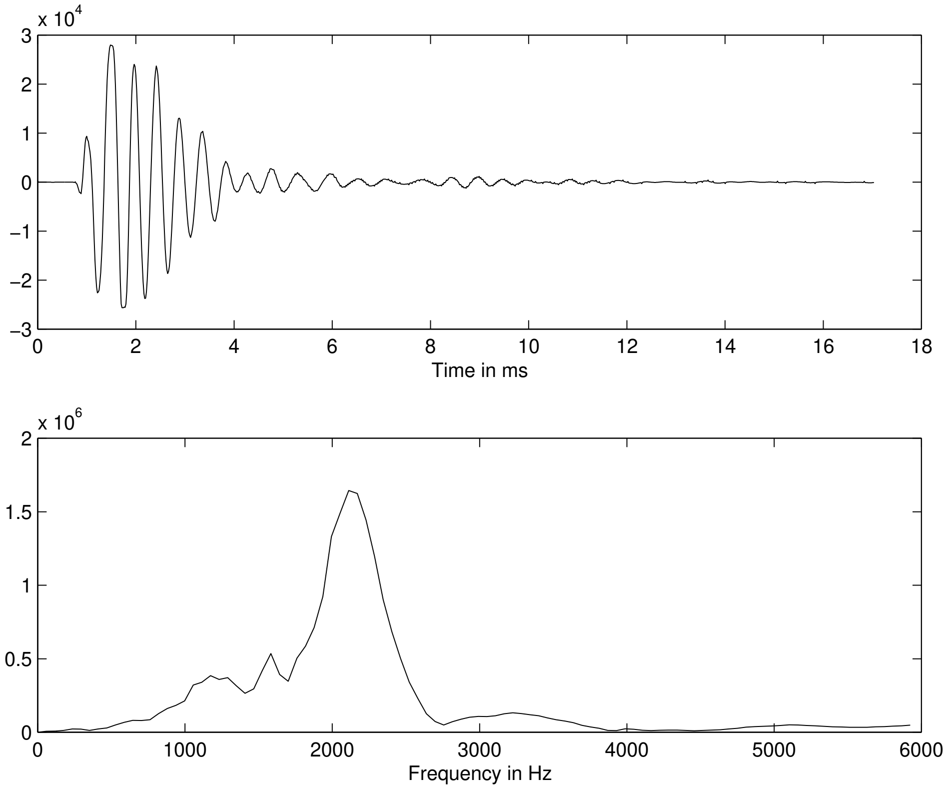

Figure 4.25: Example of a received signal from the sand box without target. MST is transmitter and Terr is receiver. The MST-Terr distance is 16 cm, and the source electrical signal 2 kHz, two cycles. Top: Echo signal. Bottom: Spectrum amplitude.

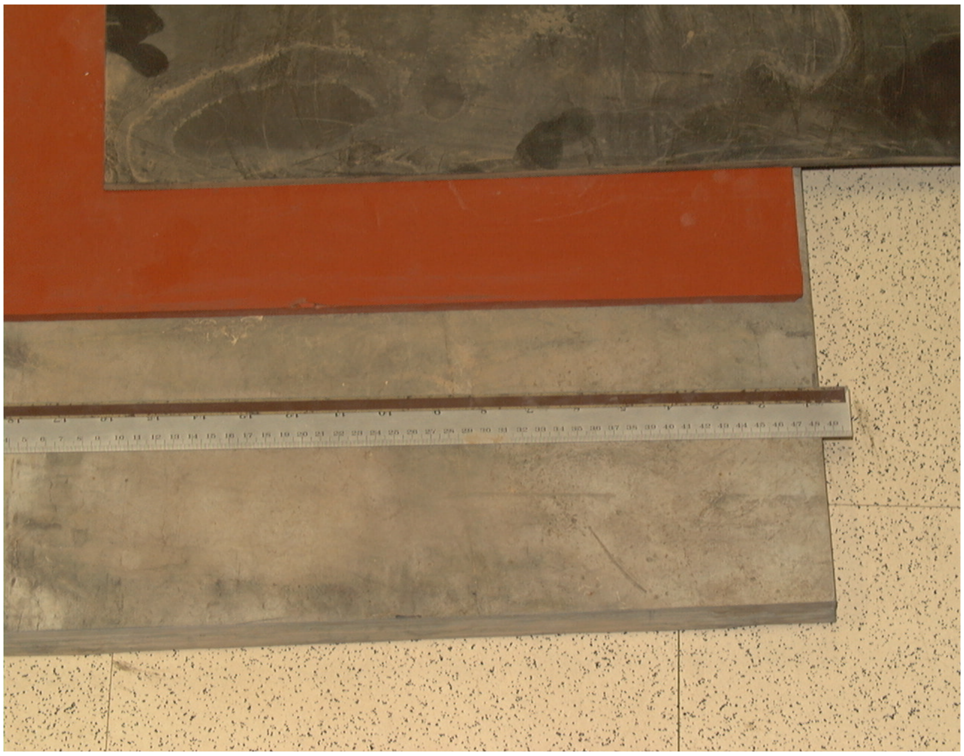

Figure 4.26: Materials used to modify the coupling between the transducers. Top: Neoprene, 6 mm thick. Middle: Red SOAB (Wallgone, Consumer Usage Laboratories, Inc.), 1 cm thick. Bottom: Silver SOAB (Goodrich & Co.), 2.5 cm thick.

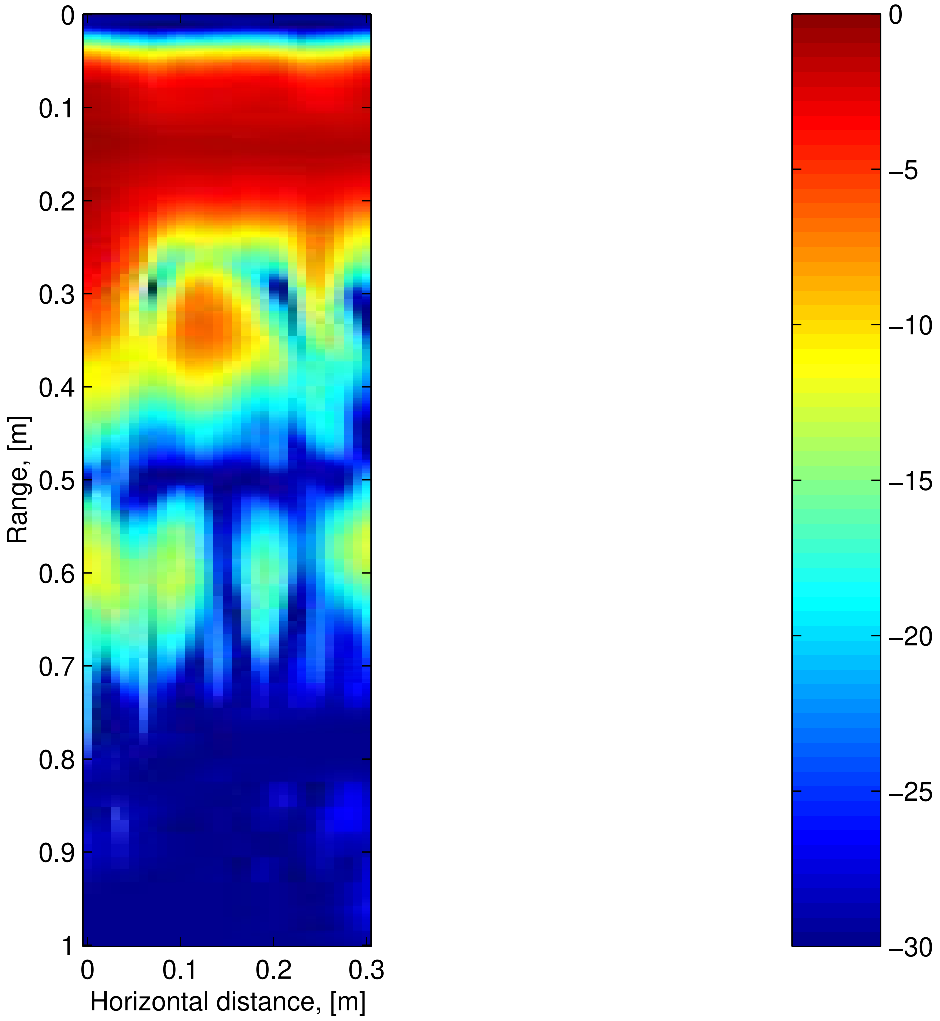

Figure 4.27: B-mode image in sandbox with a small plate buried 22 cm deep. Silver SOAB was used. MST is transmitter and Terr is receiver. The MST-Terr distance is 13 cm, and the source electrical signal is 2 kHz, two cycles.

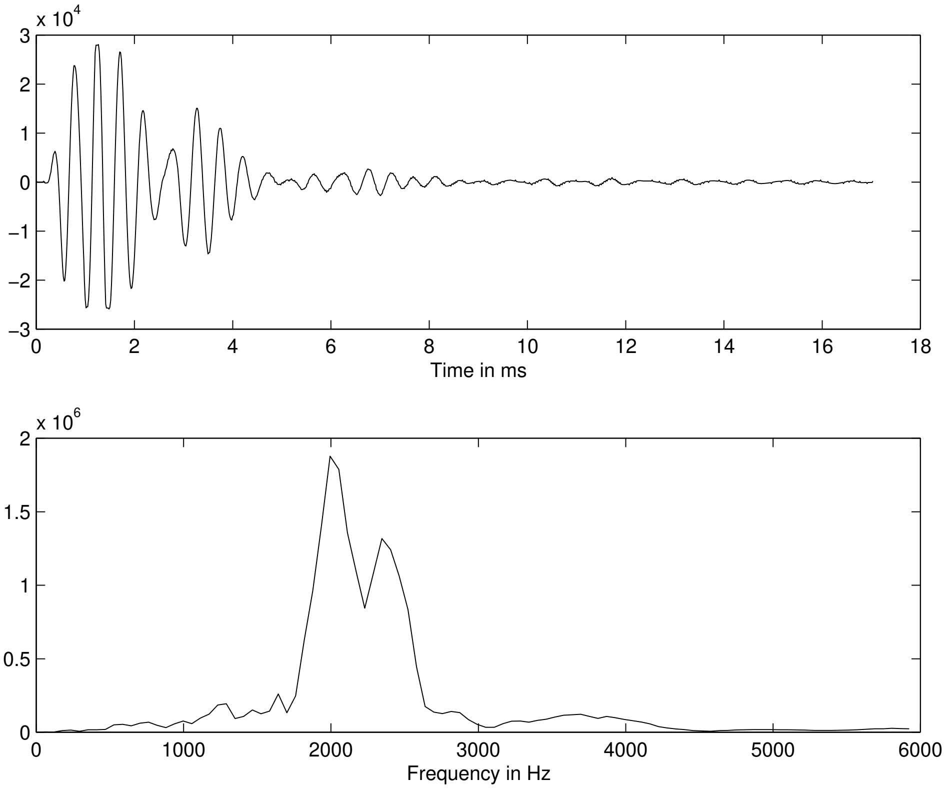

Figure 4.28: Example of a received signal from over a plate buried 22 cm deep. Silver SOAB was used. MST is transmitter and Terr is receiver. The MST-Terr distance is 13 cm, and the source electrical signal is 2 kHz, two cycles. Top: Echo signal. Bottom: Spectrum amplitude.

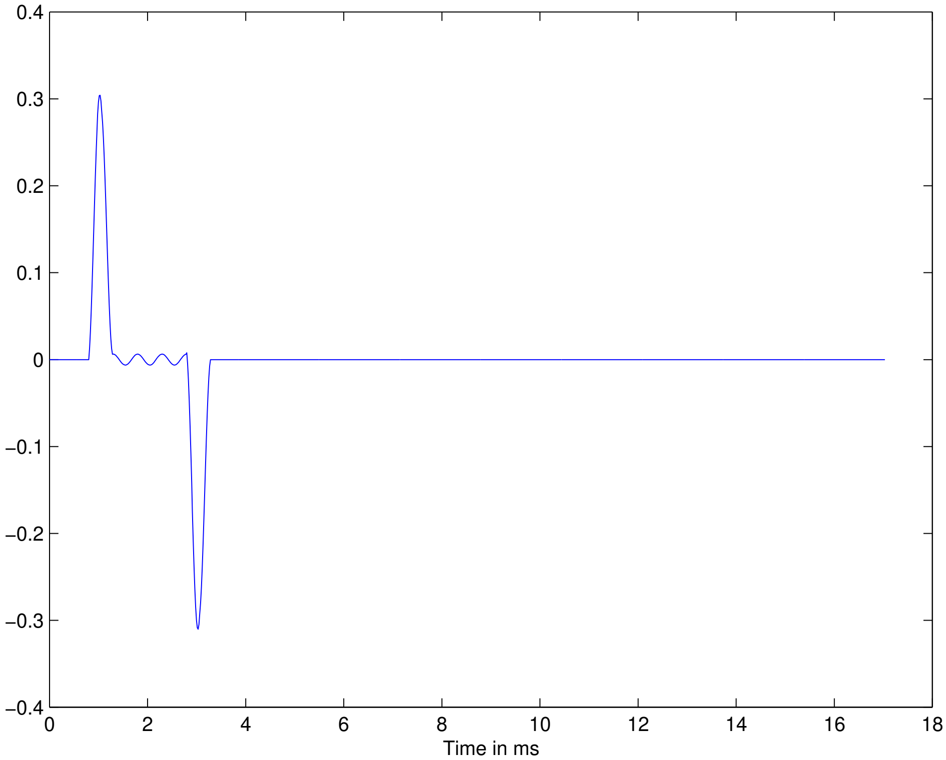

Figure 4.29: Summation of 16 phase-shifted (spreading one wavelength) four-cycle sine waves each with unit amplitude.

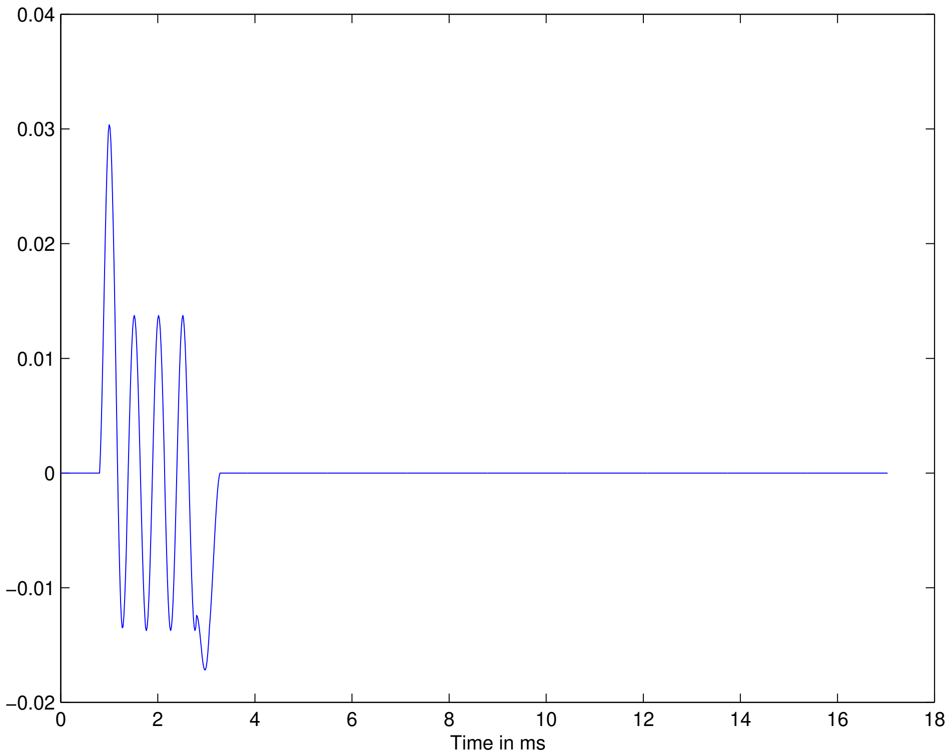

Figure 4.30: Summation of 16 phase-shifted (spreading one wavelength) and attenuated four-cycle sine waves each with unit amplitude.

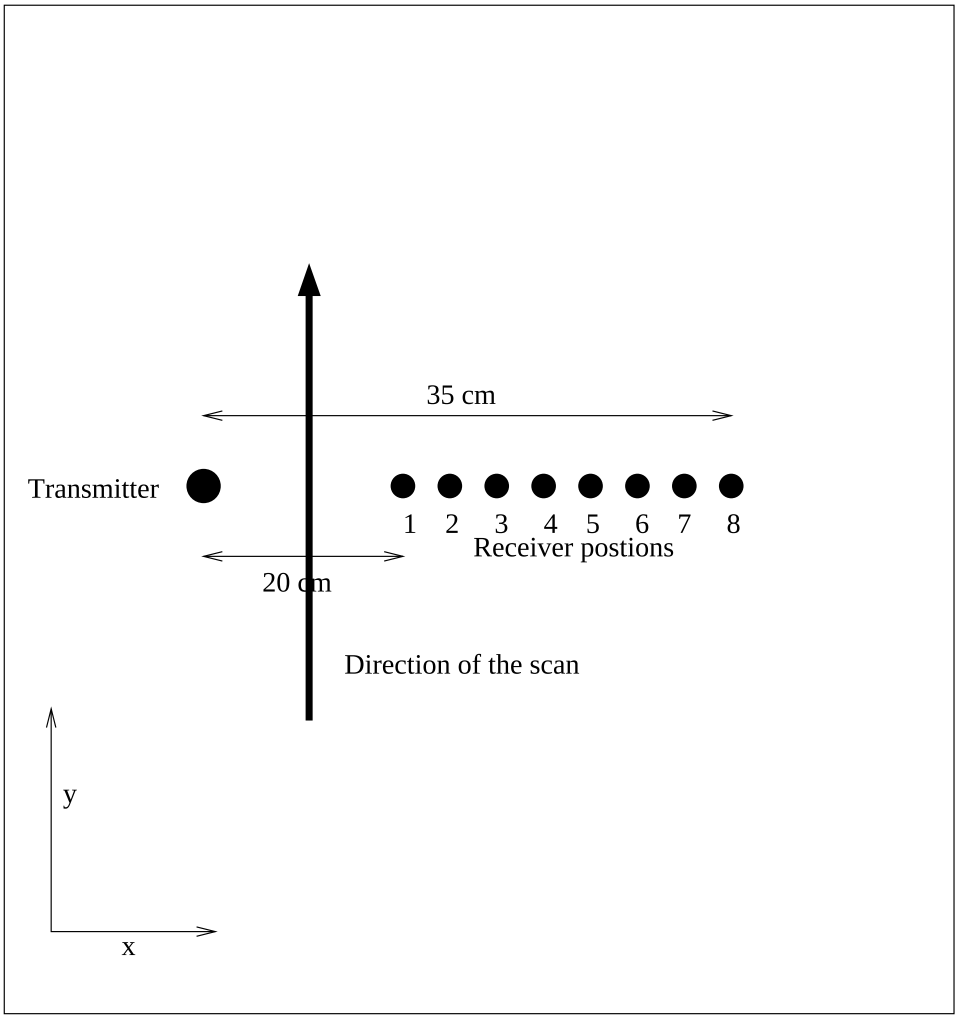

Figure 4.31: Scan scheme used to try to mitigate the direct wave. View from the top. For each transmitter position, eight received signals were acquired. The center-to-center distance from the transmitter to the receiver varied from 20 cm to 35 cm.

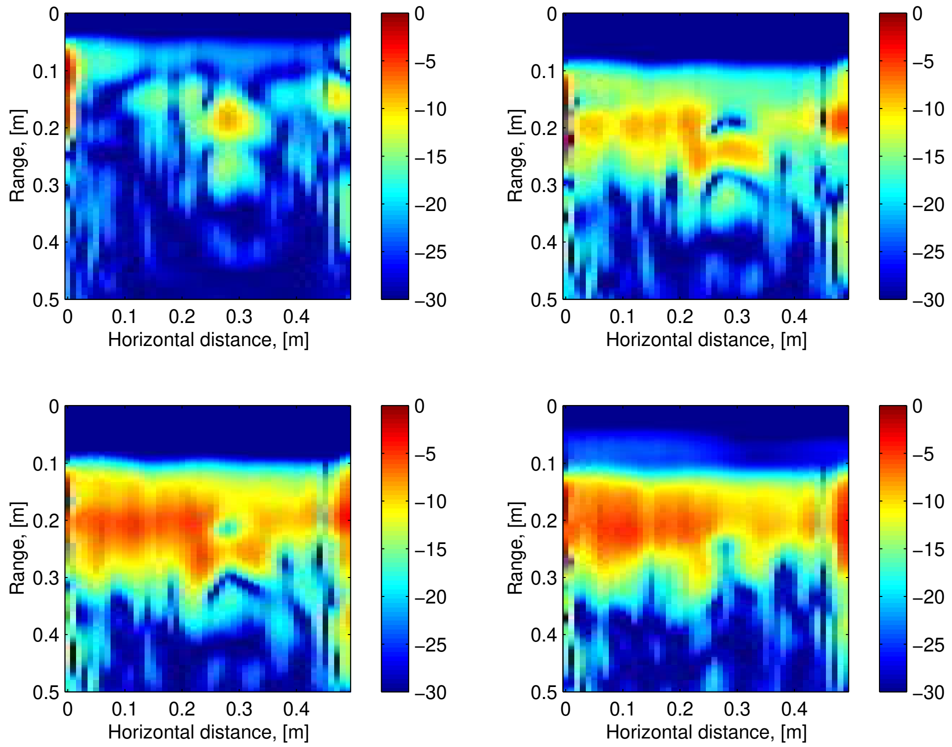

Figure 4.32: Reconstructed pictures at different depths of focus, where an eight-element receiving array covering two wavelengths of the direct wave was used. This geometry is described in Figure 4.31. MST is transmitter, Terr is receiver, and the source electrical signal is 2 kHz, two cycles. The target was a small plate buried at a depth of around 18 cm, whose longest side was across the direction of scanning. The focus depths from left to right and from top to bottom are 0, 9 cm, 18 cm, and ∞.

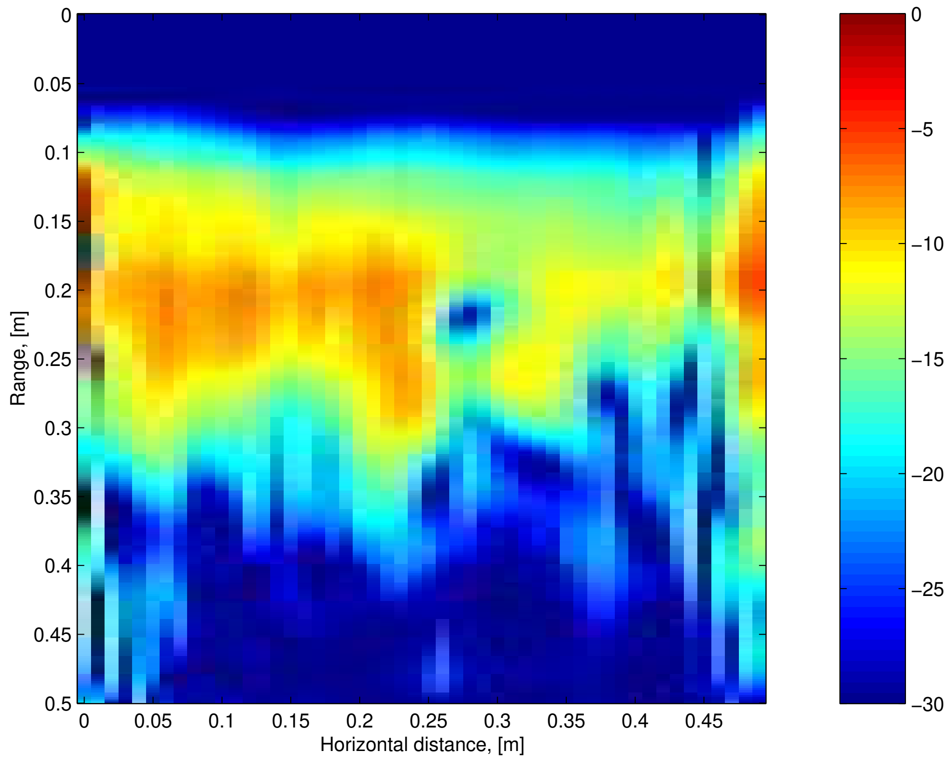

Figure 4.33: Reconstructed picture using DF at 20 different depths, where an eight-element receiving array covering two wavelengths of the direct wave was used. This geometry is described in Figure 4.31. MST is transmitter, Terr is receiver, and the source electrical signal is 2 kHz, two cycles. The target was a small plate buried at a depth of around 18 cm, whose longest side was across the direction of scanning.